Role of oceanic ozone deposition in explaining short-term variability of surface ozone at high-Arctic sites

Johannes G.M. Barten[1], Laurens N. Ganzeveld[1], Gert-Jan Steeneveld[1], and Maarten C. Krol[1,2]

[1]Wageningen University, Meteorology and Air Quality Section, Wageningen, the Netherlands
[2]Institute for Marine and Atmospheric Research Utrecht, Utrecht University, Utrecht, the Netherlands

Correspondence: Johannes G.M. Barten (sjoerd.barten@wur.nl)

Abstract. Dry deposition is an important removal mechanism for tropospheric ozone (O_3). Currently, O_3 deposition to oceans in atmospheric chemistry and transport models (ACTMs) is generally represented using constant surface uptake resistances. This is despite the fact that considering the role of solubility, waterside turbulence and O_3 reacting with ocean water reactants such as iodide results in substantial spatiotemporal variability in O_3 deposition and concentrations in marine boundary layers.

5 We hypothesize that O_3 deposition to the Arctic ocean, having a relatively low reactivity, is overestimated in current models with consequences for tropospheric concentrations, lifetime and long-range transport of O_3. In this study, we investigate the impact of the representation of oceanic O_3 deposition to the simulated magnitude and spatiotemporal variability in Arctic surface O_3.

We have integrated the Coupled Ocean-Atmosphere Response Experiment Gas transfer algorithm (COAREG) into the mesoscale

10 meteorology and atmospheric chemistry model Polar-WRF-Chem (WRF) which introduces a dependence of O_3 deposition on physical and biogeochemical drivers of oceanic O_3 deposition. We have also reduced the O_3 deposition to sea ice and snow. Here, we evaluate the performance of WRF and the CAMS reanalysis data against hourly-averaged surface O_3 observations at 25 sites (latitudes > 60 ºN) including the Arctic Summer Cloud Ocean Study (ASCOS) campaign observations. This is the first time such a coupled modelling system has been evaluated against hourly observations at Pan-Arctic sites to study the sensitivity

15 of the deposition scheme to the magnitude and short-term temporal variability in Arctic surface O_3. We also analyze the impact of nudging WRF to the synoptic conditions from the ECMWF ERA5 reanalysis data on simulated Arctic meteorology and comparison of observed and simulated O_3 concentrations.

We show that the more mechanistic representation of O_3 deposition over oceans and reduced snow/ice deposition improves simulated Arctic O_3 mixing ratios both in terms of magnitude but also regarding observed temporal variability. Using the newly

20 implemented approach, O_3 deposition velocities have been simulated in the order of 0.01 cm s^{-1} compared to $\sim$0.05 cm s^{-1} in the constant surface uptake resistance approach. The simulated monthly-mean spatial variability in the mechanistic approach (0.01 to 0.018 cm s^{-1}) expresses the sensitivity to chemical enhancement with dissolved iodide whereas the temporal variability (up to $\pm$ 20% around the mean) expresses mainly differences in waterside turbulent transport. The bias for all observational sites above 70 ºN reduced from -7.7 ppb to 0.3 ppb with nudging and the revision to ocean and snow/ice deposition. Our study

25 confirms that O_3 deposition to high-latitude oceans and snow/ice is generally overestimated in ACTMs. We recommend that a

mechanistic representation of oceanic O_3 deposition should be used in ACTMs to improve the representation of Arctic surface O_3 concentrations in terms of magnitude and short-term temporal variability.

1 Introduction

Tropospheric Ozone (O_3) is the third most important greenhouse gas and a secondary air pollutant negatively affecting human health (Nuvolone et al., 2018), plant growth (Ainsworth et al., 2012) and artificial materials such as rubber (Lee et al., 1996) due to its oxidative character. O_3 shows a large spatiotemporal variability due to its relatively short lifetime (3-4 weeks) in the free troposphere compared to other greenhouse gases. Its main sources are chemical production and entrainment from the stratosphere. Its main sinks are chemical destruction and deposition to the Earth's surface (Young et al., 2018; Tarasick et al., 2019). Understanding the Arctic O_3 budget is of particular interest because its remote location implies that anthropogenic sources and sinks are generally absent. This makes these Arctic O_3 observations excellent indicators for global trend analysis (Helmig et al., 2007b; Gaudel et al., 2020; Cooper et al., 2020). In the Arctic, routine tropospheric O_3 observations indicate an increasing trend up to the early 2000s which is leveling off (Oltmans et al., 2013; Cooper et al., 2014) or decreasing at individual sites (Cooper et al., 2020) in the last decade. This upward trend can be attributed to increased emissions of precursors in the mid-latitudes (Cooper et al., 2014; Lin et al., 2017), but also changes in O_3 deposition to vegetation as a result of droughts and heatwaves (Lin et al., 2020) and stratosphere-to-troposphere transport may have played a role (Pausata et al., 2012). Local emissions of precursors are expected to become an important source of Arctic O_3 concentrations due to the warming Arctic climate and increasing local economic activity (Marelle et al., 2016; Law et al., 2017). This underlines the need for understanding the sources and sinks of Arctic tropospheric O_3 and to accurately represent them in atmospheric chemistry and transport models (ACTMs).

On the global scale, dry deposition accounts for $\sim$25% of the total sink term (Lelieveld and Dentener, 2000) in ACTM simulations and is especially important for the O_3 budget in the Atmospheric Boundary Layer (ABL) because it occurs at the Earth's surface (Kavassalis and Murphy, 2017; Lin et al., 2019, 2020). Dry deposition in ACTMs is often represented as a resistance in series approach (Wesely, 1989). In this approach the total resistance r_t is the sum of three serial resistances: the aerodynamic resistance (r_a) representing turbulent transport to the surface, the quasi-laminar sub layer resistance (r_b) representing diffusion close to the surface and the surface resistance (r_s) expressing the efficiency of removal by the surface. The dry deposition velocity (V_d) is then evaluated as the reciprocal of r_t. The r_a term is independent of the chemical species and mainly depends on the stability of the atmosphere and friction velocity (u$_*$) (Padro, 1996; Toyota et al., 2016). The r_b term also scales with u$_*$ and varies with the diffusivity of the chemical species (Wesely and Hicks, 2000). For very soluble or reactive species such as nitric acid uptake by the ocean water is very fast (i.e r_s of $\sim$0 s m^{-1}) implying that the other resistances determine r_t and thus V_d. Less soluble gases like O_3 have a high r_s, in comparison to the relatively small $r_a + r_b$ term, that dominates the magnitude of the O_3 dry deposition velocity (V_{d,O_3}). Thus, accurately representing the surface uptake efficiency of O_3 is crucial.

Observed O_3 deposition to oceans (e.g. Chang et al., 2004; Clifford et al., 2008; Helmig et al., 2012) and coastal waters (e.g. Gallagher et al., 2001) is relatively slow ($\sim$0.01-0.1 cm s^{-1}), especially compared to observed maximum V_{d,O_3} for forests up to

2 cm s^{-1} (Fan et al., 1990). However, it plays a large role in the total O$_3$ deposition budget due to the large surface area of water
bodies (Ganzeveld et al., 2009; Hardacre et al., 2015). Recent experimental and modelling studies indicate the spatiotemporal
variability in oceanic O$_3$ uptake efficiency (Ganzeveld et al., 2009; Helmig et al., 2012; Luhar et al., 2018). However, most
ACTMs often still use a constant O$_3$ surface uptake efficiency of 2000 cm s^{-1} to water bodies, proposed by Wesely (1989), re-
sulting in a simulated ocean V_{d,O_3} of $\sim$0.05 cm s^{-1}. The observed V_{d,O_3} shows a larger variability including also a dependency
on wind speed and Sea Surface Temperature (SST) (Helmig et al., 2012). The dependency on wind speed also expresses an
enhancement of O$_3$ deposition due to waterside turbulence (Fairall et al., 2007). This turbulence driven enhancement is comple-
mented by a strong chemical enhancement of oceanic O$_3$ deposition associated with its chemical destruction through oxidation
of ocean water reactants such as dissolved iodide and dissolved organic matter (DOM) (Chang et al., 2004). Mechanistic O$_3$
deposition representations in models include the physical and biogeochemical processes related to the exchange and destruc-
tion of O$_3$ in surface waters (Fairall et al., 2007, 2011; Ganzeveld et al., 2009; Luhar et al., 2017, 2018). Dissolved iodide is
deemed to be the main reactant of O$_3$ in surface waters (Chang et al., 2004) and therefore often applied in these representa-
tions. Some studies only consider dissolved iodide as a reactant (Luhar et al., 2017; Pound et al., 2019) whereas Ganzeveld
et al. (2009) also included DOM as one reactant contributing to the chemical enhancement of oceanic O$_3$ deposition. However,
the role of DOM in oceanic O$_3$ deposition remains difficult to quantify which appears to be mainly addressed by controlled
laboratory experiments or O$_3$ flux measurements at sites with elevated DOM water concentrations. Nevertheless, application
of these more mechanistic ocean O$_3$ deposition representations illustrated the importance of a more explicit representation of
O$_3$ dry deposition in ACTMs, not only regarding the impact on marine ABL O$_3$ concentrations and budget, but also to consider
potentially important feedback mechanisms. For instance, consideration of the mechanisms that ultimately determine the effi-
ciency of uptake and destruction of O$_3$ in ocean surface waters might also explain the release of halogen compounds into the
ABL (Prados Roman et al., 2015). These halogens, in turn, are involved in O$_3$ depletion and therefore reduce further uptake
and destruction of O$_3$ in ocean surface waters implying existence of a negative feedback mechanism.

Up until now, earlier studies on global scale oceanic O$_3$ deposition (Ganzeveld et al., 2009; Luhar et al., 2017) mainly relied
on the evaluation of monthly mean surface O$_3$ observations (Pound et al., 2019). The implementation of these mechanistic
exchange methods in ACTMs, in particular the method proposed by Luhar et al. (2018) using a two-layer model representation
(compared to a bulk layer version by Ganzeveld et al. (2009)), results in a $\sim$50% reduction of the global mean V_{d,O_3} which
affects the tropospheric O$_3$ burden (Pound et al., 2019). The mechanistic representation in Pound et al. (2019) especially results
in a simulated decrease in V_{d,O_3} to cold polar waters with relatively low reactivity. Simulated V_{d,O_3} can be as low as 0.01 cm
s^{-1} compared to the commonly applied V_{d,O_3} of 0.05 cm s^{-1} in the constant surface uptake resistance approach (Pound et al.,
2019). However, the hypothesized deposition reduction to cold waters is expected to substantially affect Arctic ABL O$_3$ con-
centrations on shorter timescales and potentially improve operational Arctic O$_3$ forecasts, e.g. the air quality forecasts by the
Copernicus Atmosphere Monitoring Service (CAMS) (Inness et al., 2019).

The evaluation of simulated oceanic O$_3$ deposition in the Arctic is hampered by a lack of O$_3$ ocean-atmosphere flux observa-
tions. Hence, evaluation of simulated O$_3$ deposition relies on evaluation of surface O$_3$ concentrations not only regarding the
simulated and observed magnitude but in particular on the highly resolved temporal variability. We hypothesize that on the

daily and diurnal timescales these concentrations are largely controlled by temporal variability in the main physical drivers of

95 oceanic O_3 deposition, e.g. atmospheric and waterside turbulence. Chemical enhancement of, e.g., iodide to O_3 deposition is anticipated to control more the long-term (weeks-months) baseline level of V_{d,O_3} associated with anticipated long-term (e.g. seasonal) changes in ocean water biogeochemical conditions (Sherwen et al., 2019). This evaluation of Arctic spatiotemporal O_3 concentrations aims to better understand sinks, processes, feedbacks and impacts of Arctic air pollution (Arnold et al., 2016) and the role of long-range transport (e.g. Thomas et al., 2013; Marelle et al., 2018) versus local sources (e.g. Marelle et al.,

100 2016; Law et al., 2017; Schmale et al., 2018). Furthermore, the projected opening of the Arctic ocean, as a result of climate change, urges to improve our understanding of Arctic ocean-atmosphere exchange. This study focuses on the ocean-atmosphere exchange of O_3, but follow-up studies are planned with a focus on ocean-atmosphere exchange and ABL concentrations of other trace gases such as dimethylsulfide (DMS), which enhances cloud formation and is involved in many feedback mechanisms (Mahmood et al., 2019).

105 We aim to identify and quantify the impact of a mechanistic representation of O_3 deposition in explaining observed hourly Arctic surface O_3 concentrations, both in terms of magnitude and temporal variability. A mesoscale coupled meteorology-atmospheric chemistry model is evaluated against a large dataset of pan-Arctic O_3 observations at a high resolution (hourly) timescale for the end-of-summer 2008. Having a much higher spatial and temporal resolutions compared to other global modelling studies we aim to better capture the role of spatiotemporal variability in O_3 deposition in explaining observed surface

110 O_3 concentrations particularly regarding temporal variability. We also indicate the role of meteorology in simulating these O_3 concentrations by nudging the simulated synoptic conditions towards an atmospheric reanalysis dataset. Section 2 describes the adjustments to the deposition scheme in the mesoscale ACTM, further model setup and observational datasets. Section 3 presents the main results of the study which are further discussed in Sect. 4. This manuscript is finalized with the conclusions in Sect. 5.

2 Methods

115

2.1 Regional coupled meteorology-chemistry model

We use the Weather Research and Forecasting model (v4.1.1) coupled to chemistry (Chem) (Grell et al., 2005) and optimized for Polar regions (Hines and Bromwich, 2008). Polar-WRF-Chem (hereafter: WRF) is a non-hydrostatic mesoscale numerical weather prediction and atmospheric chemistry model used for operational and research purposes. Figure 1 shows the selected

120 study area including the locations of surface O_3 observational sites selected for this study (more information in Sect. 2.3). WRF is set up with a polar projection centered at 90°N, 250×250 horizontal grid points (30×30 km resolution) and 44 vertical levels up to 100 hPa, with a finer vertical grid spacing in the ABL and lower troposphere. The simulation period is 08-August-2008 to 07-September-2008 including three days of spin-up. This end-of-summer 2008 period is chosen: 1) to limit the role of active halogen chemistry during springtime (Pratt et al., 2013; Thompson et al., 2017; Yang et al., 2020) and 2) the additional

125 availability of O_3 observations in the high Arctic over sea ice from the ASCOS campaign (Paatero et al., 2009). The ECMWF ERA5 meteorology (0.25°×0.25°) (Hersbach et al., 2020) and CAMS reanalysis chemistry (0.75°×0.75°) (Inness et al., 2019)

products are used for the initial and boundary conditions. Boundary conditions, SSTs and sea ice fractions are updated every three hours to these reanalysis products to allow for the sea ice retreat during the simulation. Other relevant parameterization schemes and emission datasets have been listed in Tab. A1 and are mostly based on Bromwich et al. (2013).
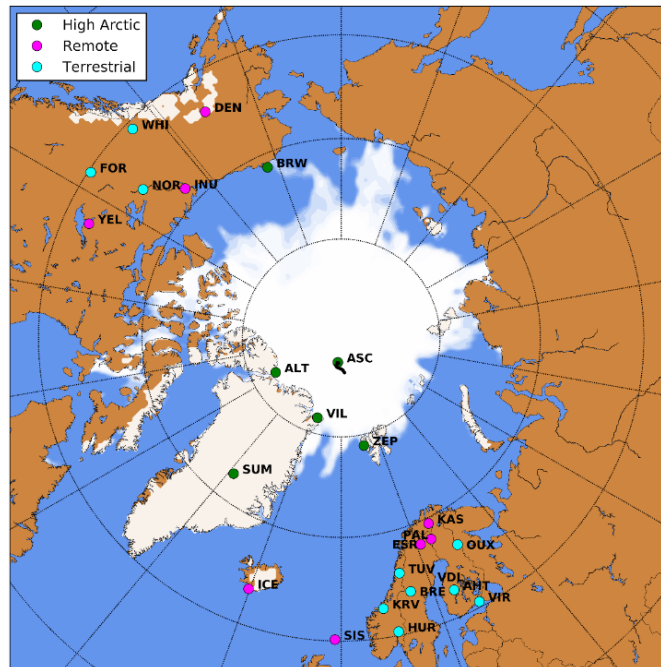

Figure 1. WRF domain including sea ice and snow cover at the start of the simulation. Locations with surface observations O_3 are indicated in green (High Arctic), magenta (Remote) and cyan (Terrestrial) (see Sect. 2.3). The drifting path of the ASCOS campaign during the simulation is indicated with the black line.

2.1.1 Nudging to ECMWF ERA5

The first WRF simulation, without any adjustments to O_3 deposition, indicated that WRF was misrepresenting the temporal variability in surface O_3 observations, most prominently starting from a few days into the simulation. We hypothesize that this misrepresentation is caused by deviations in the synoptic conditions in the free running WRF simulation. Hence, WRF results are compared against the observations from the Advanced Microwave Scanning Radiometer - Earth Observing System (AMSR-E) sensor on NASA's Aqua satellite. The near surface wind speeds above oceans from the Daily Level-3 data product are used with a spatial resolution of $0.25° \times 0.25°$ (Wentz and Meissner, 2004).

Figure 2 shows the temporal evolution in the bias (WRF minus AMSR-E) and Mean Absolute Error (MAE) of the daily and ocean grid box averaged 10-m wind speeds. Although the first days there is no clear bias, later in the simulation we find a persistent positive wind speed bias indicating that WRF overestimates the wind speeds above the Arctic ocean. During the first days the MAE amounts to ~1.5 m s^{-1}, while later in the simulation the MAE reaches 2.5-3.0 m s^{-1}. To overcome the impact of

5

this deficiency on our O_3 budget study, nudging is applied to ensure a fair model evaluation with observations. Hence, WRF is nudged every three hours to the ECMWF ERA5 humidity, temperature and wind fields in the free troposphere with nudging coefficients of $1\cdot10^{-5}$ s^{-1}, $3\cdot10^{-4}$ s^{-1} and $3\cdot10^{-4}$ s^{-1}, respectively. In Sect. 3.3 the impact of nudging on simulated surface O_3 is further analysed.
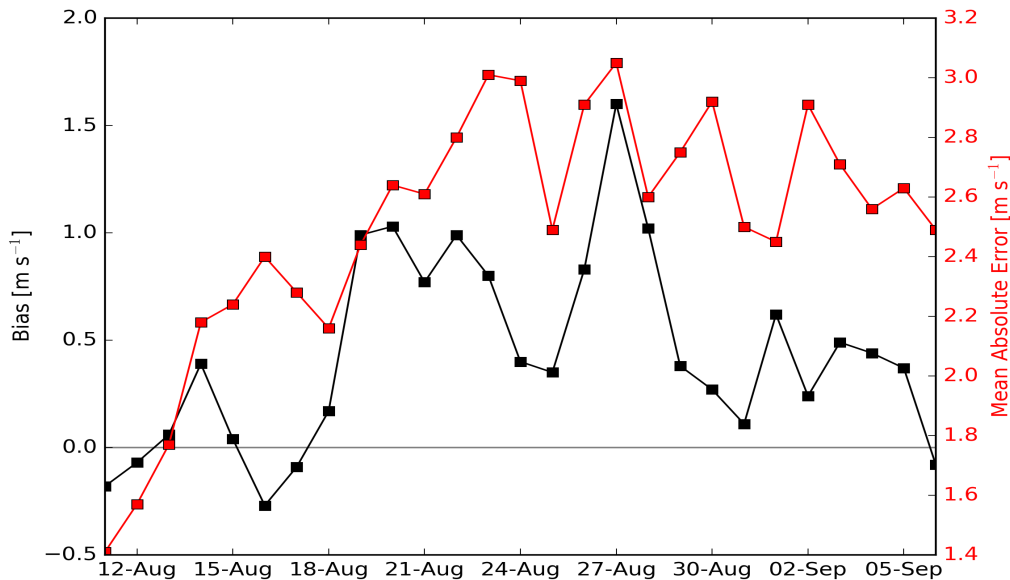
Figure 2. Temporal evolution of the bias (WRF minus AMSR-E, black) [m s^{-1}] and Mean Absolute Error (MAE, red) [m s^{-1}] of 10-m wind speeds above oceans for the period of 11-Aug to 6-Sep 2008. Note that the right y-axis starts at 1.4 m s^{-1}.

2.2 Representation of ocean-atmosphere gas exchange

The Coupled Ocean-Atmosphere Response Experiment (COARE) (Fairall et al., 1996) has been developed to study physical exchange processes (sensible heat, latent heat and momentum) at the ocean-atmosphere interface. Later, COARE has been extended to include the exchange of gaseous species such as O_3, dimethyl sulfide (DMS) and carbon dioxide (CO_2) (Fairall et al., 2011). Many studies have used the COARE Gas transfer algorithm (COAREG) in combination with eddy covariance measurements to study the effects of wind speed and sea state on ocean-atmosphere gas exchange (e.g. Helmig et al. (2012), Blomquist et al. (2017), Bell et al. (2017), Porter et al. (2020)). Furthermore, the COAREG algorithm has also been previously used in global O_3 modelling studies Ganzeveld et al. (2009). The choice for COAREG as ocean-atmosphere exchange parameterization is further motivated by the consistent coupling with other species such as DMS.

Here we use COAREG version 3.6, which is extended with a two-layer scheme for surface resistance compared to the previous version described by Fairall et al. (2007, 2011). The two-layer scheme is similar to Luhar et al. (2018) building upon a first

application of a 1-layer version of COAREG by Ganzeveld et al. (2009). In that study, chemical enhancement of ocean O_3 deposition by its reaction with iodide was considered using a global climatology of ocean surface water concentrations of nitrate serving as a proxy for oceanic iodide concentrations (Γ_{aq}^-), the compound that is generally deemed to be the most significant reactant for O_3 in ocean water (Chang et al., 2004). Besides nitrate, satellite-derived chlorophyll-α concentrations have been used as a proxy for Γ_{aq}^- (Oh et al., 2008). Since then, alternative parameterizations of oceanic Γ_{aq}^- have been proposed (e.g. MacDonald et al., 2014) using SST as a proxy for this reactant. In COAREG, chemical reactivity of O_3 with Γ_{aq}^- is present through the depth of the oceanic mixing layer. O_3 loss by waterside turbulent transfer is negligible in the top water layer (few micrometers), but is accounted for in the underlying water column. The waterside turbulent transfer term is especially relevant for relatively cold waters because the chemical enhancement term is then relatively low (Fairall et al., 2007; Ganzeveld et al., 2009; Luhar et al., 2017). The last two important waterside processes that determine the total O_3 deposition are molecular diffusion and solubility of O_3 in seawater which both depend on the SST. In Appendix B we list the formulation of the air- and waterside resistance terms in the COAREG routine applied in this study and show the sensitivity to the environmental factors wind speed, SST and Γ_{aq}^- for typical Arctic conditions.

In this study, the COAREG algorithm is coupled such that WRF provides the meteorological and SST input for the COAREG routine. In turn, the COAREG calculated ocean-atmosphere exchange velocities are used in the WRF model to calculate the oceanic O_3 deposition flux replacing the default oceanic O_3 deposition fluxes calculated by the Wesely (1989) scheme reflecting use of the default constant r_s of 2000 s m^{-1}. For grid boxes with fractional sea ice cover, COAREG replaces the Wesely deposition scheme for the fraction that is ice free. Note that in this study, only O_3 ocean-atmosphere exchange is represented by COAREG not having modified simulations of ocean-atmosphere exchange of other compounds (e.g. DMS).

Moreover, we apply the monthly-mean Γ_{aq}^- distribution by Sherwen et al. (2019) ($0.125° \times 0.125°$ resolution) which applies a machine learning approach, namely the Random Forest Regressor algorithm (Pedregosa et al., 2011), using various physical and chemical variables such as SST, nitrate and chlorophyll-α. This distribution replaces the previously applied Γ_{aq}^- estimations only using SST (Chance et al., 2014; MacDonald et al., 2014). At high latitudes, these Γ_{aq}^- distributions are highly uncertain due to the limited number of observations. However, the choice for Sherwen et al. (2019) is motivated by the most accurate representation of observed Γ_{aq}^- on the global scale. Figure C1 shows the spatial distribution of Γ_{aq}^- used in the calculation of the O_3 deposition velocities of COAREG coupled to the WRF model. Using the Sherwen et al. (2019) distribution for August/September we found relatively high Γ_{aq}^- concentrations ranging between 30 nM and 80 nM for the open oceans up to 130 nM in coastal waters. In MacDonald et al. (2014) and Chance et al. (2014), Γ_{aq}^- is solely a function of SST which leads to Γ_{aq}^- in the order of 5 to 50 nM and thus low reactivity and O_3 deposition velocities.

2.2.1 Deposition to snow and ice

Reported atmosphere-snow gas exchange spans a wide range of observed O_3 deposition velocities. Some studies even report episodes of negative deposition fluxes (emissions) over snow or sea ice (Zeller, 2000; Helmig et al., 2009; Muller et al., 2012). Clifton et al. (2020b) recently summarized observed O_3 deposition velocities to snow having a range of -3.6 to 1.8 cm s^{-1} with most of the observations indicating a deposition velocity between 0 and 0.1 cm s^{-1} for multiple snow covered surfaces

190 (e.g. grass/forest/sea-ice). Generally, ozone concentrations in the interstitial air of the snowpack is lower than in the air above making it a not a direct source of O_3 in terms of emissions (Clifton et al., 2020b). However, the emissions of O_3 precursors from the snowpack can enhance O_3 production in the very stable atmosphere above the snowpack (Clifton et al., 2020b). Helmig et al. (2007a) investigated the sensitivity of a chemistry and tracer transport model to the prescribed O_3 deposition velocity and found best agreement between modelled and observed O_3 concentrations by applying deposition velocities in the

195 order of 0.00-0.01 cm s^{-1}. Following Helmig et al. (2007a) we have increased the O_3 surface uptake resistance (r_s) for snow and ice land use classes to 10^4 s m^{-1}. This corresponds to total deposition velocities of ≤ 0.01 cm s^{-1}, which is a reduction of $\sim 66\%$ compared to the Wesely deposition routine that is the default being applied in WRF (Grell et al., 2005). Effects of this modification are further examined in Sect. 3.1.

2.3 Observational data of surface ozone

200 The new modelling setup, including nudging to ECMWF ERA5 and the revised O_3 deposition to snow, ice and oceans, is evaluated against observational data of pan-Arctic surface O_3 concentrations. We expect that the different representation of O_3 deposition mostly affects O_3 concentrations in the ABL. Therefore, we evaluate our simulations against hourly averaged surface O_3 observations from 25 measurement sites above 60 °N. These sites are further categorized in three site selections: 'High Arctic', 'Terrestrial' and 'Remote'. High Arctic refers to sites having latitudes > 70 °N and for which we expect that

205 the deposition footprint is a combination of ocean and sea-ice (e.g. Helmig et al., 2007b). The Terrestrial sites are located below 70 °N and show a clear diurnal cycle in observed O_3 (e.g. Chen et al., 2018). These diurnal cycles are governed by a combination of emissions of precursors, but also the anticipated larger diurnal cycle in O_3 deposition (Zhou et al., 2017) to, e.g., vegetated surfaces and a stronger diurnal cycle in turbulent mixing conditions and ABL dynamics. These are in all aspects different from sites that have an ocean/sea-ice footprint where we expect low emissions of precursors, no clear diurnal cycle

210 in O_3 deposition and a weaker diurnal cycle in ABL dynamics (Van Dam et al., 2015). In this study, the criterion is that the average observed minimum nighttime mixing ratio is > 8 ppb smaller than the average observed maximum daytime mixing ratio during the ~ 1 month of simulation. This criterion is based on a preparatory analysis of the observational data, footprint and site characteristics. The Remote sites have been identified as such based on their location below 70 °N and showing no clear diurnal cycle in O_3 concentrations. The analysis also includes the observations during the Arctic Summer Cloud Ocean

215 Study (ASCOS) campaign, when the icebreaker Oden was located in the Arctic sea ice (Tjernstrom et al., 2012). In total, 25 surface O_3 measurement sites are included (Fig. 1) of which 6, 8 and 11 sites are characterized High Arctic, Remote and Terrestrial sites, respectively. A full list of available measurement sites is available in Tab. D1.

2.4 Overview of performed simulations

In total, we perform three simulations. The first WRF simulation (DEFAULT) is a run without any adjustments to the code as

220 described in Sect. 2.1. The second simulation (NUDGED) includes nudging of the synoptic conditions to the ECMWF ERA5 product as described in Sect. 2.1.1. The third simulation (COAREG) includes nudging, but also includes the adjustments to the O_3 deposition to oceans as described in Sect. 2.2 and the O_3 deposition to snow and ice as described in Sect. 2.2.1. Furthermore,

we also compare our results with the the state-of-the-art CAMS global reanalysis data product (Inness et al., 2019). This product has a temporal resolution of 3 hours, a spatial resolution of 0.75°×0.75° and does not include a mechanistic representation of ocean-atmosphere O_3 exchange. CAMS assimilates satellite observations of O_3 but it does not assimilate O_3 observations from radiosondes or in situ measurement sites such as the 25 sites used in the here presented evaluation. Moreover, CAMS is being widely used for air quality forecasts and assessments but also to constrain regional scale modelling experiments such as presented in this study.

3 Results

First, we will present the spatial and temporal variation in O_3 dry deposition velocities (V_{d,O_3}) of the NUDGED and COAREG modelling setup including the effect on the total O_3 deposition budget. Subsequently we will discuss the resulting effect on the spatial distribution of the mean surface O_3 mixing ratios. Then, we will present the comparison of all WRF simulations and CAMS data with the hourly surface observations for the three site selections (High Arctic, Remote and Terrestrial). This section is finalized by the simulated and observed time series for the six High Arctic sites.

3.1 Dry deposition budgets and distribution

Figure 3a and Fig. 3b show the mean deposition velocities for the NUDGED and COAREG runs, respectively. As expected, in the NUDGED run (Fig. 3a) the mean V_{d,O_3} to oceans are in the order of 0.05 cm s⁻¹. Furthermore, the spatial distribution shows a relatively low heterogeneity and no increase in deposition velocities towards the warmer waters. The COAREG run (Fig. 3b) provides a mean V_{d,O_3} in the order of 0.01 cm s⁻¹ for the Arctic ocean > 70°N up to 0.018 cm s⁻¹ for oceans with high I^-_{aq} concentrations (Fig. C1). Simulated oceanic O_3 deposition is elevated in coastal waters (e.g. Baltic Sea and around the Bering Strait) with I^-_{aq} concentrations reaching up to 130 nM compared to 30-50 nM for the open Arctic ocean waters (Fig. C1). This highlights the sensitivity of the COAREG scheme to chemical enhancement with dissolved iodide.

Figure 3c shows the temporal variability in V_{d,O_3} for one of the grid boxes, which is in terms of temporal variability representative for the whole domain. The temporal variability in the NUDGED run is mainly governed by temporal variability in r_a. During episodes with high wind speeds (> 10 m s⁻¹), r_a becomes so small that it is negligible over the constant surface uptake resistance of 2000 s m⁻¹, corresponding to a maximum V_{d,O_3} of 0.05 cm s⁻¹. During episodes with low wind speeds (< 5 m s⁻¹), reduced turbulent transport poses some additional restriction on O_3 removal with increasing r_a which reduces the V_{d,O_3} to ∼0.04 cm s⁻¹. In the COAREG run, temporal variability in V_{d,O_3} is also governed by wind speeds that controls the waterside turbulent transport of O_3 in seawater besides atmospheric turbulent transport. For high wind speeds, the waterside turbulent transport increases (Fig. B1) and more O_3 is transported through the turbulent layers. For our simulation, we found that the temporal variability in O_3 deposition due to waterside turbulent transport can be up to ±20% around the mean. Overall, the V_{d,O_3} to oceans in the COAREG run is reduced by ∼60-80% compared to the NUDGED run. The mean V_{d,O_3} to snow and ice is reduced by ∼66%, from ∼0.03 cm s⁻¹ in the NUDGED run to ∼0.01 cm s⁻¹ in the COAREG run.

The temporal evolution in oceanic O_3 deposition velocities simulated by the COAREG run appears to be on the low side of

255 observed and elsewhere simulated V_{d,O_3} (e.g. Chang et al., 2004; Oh et al., 2008; Ganzeveld et al., 2009). Chang et al. (2004) showed that V_{d,O_3} can increase by a factor of 5 with wind speed increasing from 0 to 20 m s^{-1}. Luhar et al. (2017) (Figure 7) shows a wide range of observed and simulated sensitivities to wind speed. Observations from the TexAQS06 summer campaign in the Gulf of Mexico show a large sensitivity to 10-meter wind speeds even though the model seems unable to capture these high deposition velocities at high wind speeds (Luhar et al., 2017). However, Luhar et al. (2017) also shows that for the

260 GasEx08 campaign in the cold Southern Ocean the sensitivity of observed and simulated V_{d,O_3} to 10-meter wind speeds is very limited. This limited sensitivity is most accurately represented by the newer two-layer reactivity scheme compared to the older one-layer scheme due to a more limited interaction between chemical reactivity and waterside turbulent transport (Luhar et al., 2017). Furthermore, the variability around the mean presented in Tab. 1 (0.012 ± 0.002 cm s^{-1}) seems to correspond to Oh et al. (2008) (0.016 ± 0.0015 cm s^{-1}) 1 month simulation including O_3 removal by I^-_{aq}. In this study we show the intramonthly

265 variability in oceanic O_3 deposition which is expected to be relatively low compared to the seasonal variability which will also be driven by temporal changes in solubility and reactivity due to the seasonal changes in SST and I^-_{aq}.

By estimating the total deposition flux for the water, snow/ice and land surfaces we can quantify the total simulated O_3 deposition budget (Tab. 1) for the Arctic modelling domain. Land, not covered with snow or ice, is with 48% the dominant surface type for this specific domain setup in summer. Combined with a relatively high simulated V_{d,O_3} of ~0.45 cm s^{-1} this is the

270 most important sink, in terms of deposition, of simulated O_3 with ~135 Tg O_3 yr^{-1}. The simulated O_3 deposition budget to water bodies, covering 37% of the total surface area, contributes in the NUDGED run ~10% (15.4 Tg O_3 yr^{-1}) to the total O_3 deposition sink. In the COAREG run, this reduces to only ~3% (4.6 Tg O_3 yr^{-1}) of the total O_3 deposition sink. Simulated O_3 deposition to snow and ice, covering 15% of the total surface area, is the least important deposition sink removing 4.1 and 1.7 Tg O_3 yr^{-1} in the DEFAULT and COAREG runs respectively.
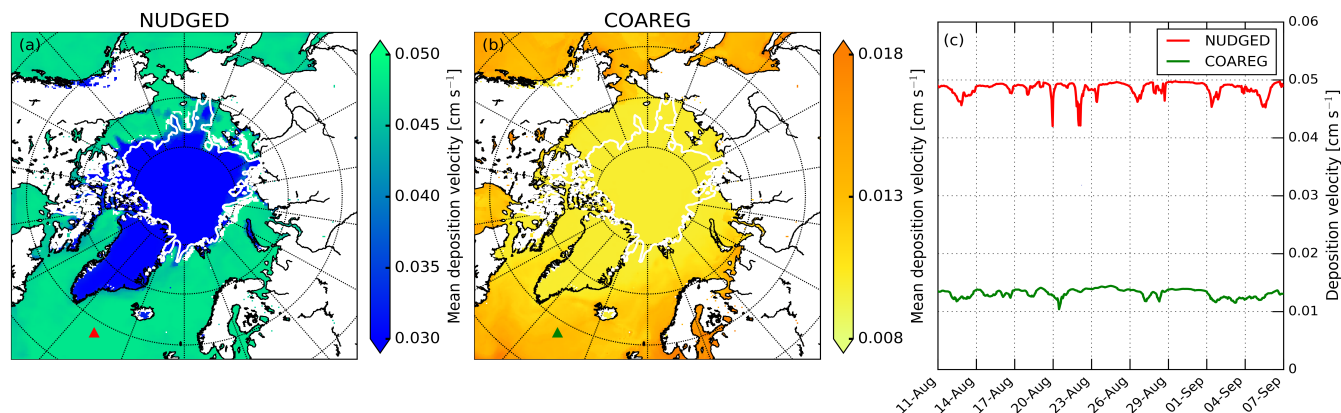
Figure 3. Spatial distribution of the mean simulated O_3 deposition velocity to snow/ice and oceans [cm s^{-1}] for the (a) NUDGED and (b) COAREG simulations and (c) temporal variation in O_3 deposition velocity [cm s^{-1}] for the NUDGED (red) and COAREG (green) simulations. The red and green markers in (a) and (b) indicate the location of the time series shown in (c). To give an indication of the sea ice extent, the white contours show the sea ice fraction of 0.5 at the start of the simulation.

Table 1. Mean simulated O_3 deposition velocity ($\pm$Standard deviation) [cm s^{-1}] and total simulated deposition budget [Tg O_3 yr^{-1}] for the NUDGED and COAREG runs to water, snow/ice and land each representing 37%, 15% and 48% of the total surface area respectively. The standard deviation gives an indication of the spatiotemporal variability in simulated O_3 deposition velocities.

		Water (37%)	Snow/Ice (15%)	Land (48%)	Total (100%)
NUDGED	Deposition velocity ($\pm$Std.) [cm s^{-1}]	0.047 ($\pm$0.003)	0.030 ($\pm$0.000)	0.449 ($\pm$0.225)	
	Deposition budget [Tg O_3 yr^{-1}]	15.4	4.1	133.4	152.9
COAREG	Deposition velocity ($\pm$Std.) [cm s^{-1}]	0.012 ($\pm$0.002)	0.010 ($\pm$0.000)	0.448 ($\pm$0.251)	
	Deposition budget [Tg O_3 yr^{-1}]	4.6	1.7	135.8	142.1

3.2 Simulated and observed monthly mean surface ozone

Figure 4 shows the spatial distribution in the simulated mean surface O_3 mixing ratios overlain with the observed mean surface O_3 mixing ratios. In the NUDGED and COAREG runs (Fig. 4a and Fig. 4b respectively) we find similar surface O_3 mixing ratios of $\sim$15-20 ppb over the Russian and Canadian/Alaskan land masses. Over Scandinavia, slightly higher surface O_3 mixing ratios of $\sim$20-25 ppb are simulated due to more anthropogenic emissions of precursors in the EDGAR emission inventory and advection of O_3 and its precursors from outside the domain. As expected, we find a limited effect of reduced deposition to water and snow/ice to the simulated mean O_3 mixing ratios over land. In general, the model appears to simulate the mean observed surface O_3 mixing ratios for the Remote and Terrestrial sites (all sites < 70 °N) generally well without clear positive or negative bias. Due to the altitude effect higher surface O_3 concentrations are simulated over Greenland even though the deposition velocity to snow and the surrounding oceans is of similar magnitude ($\sim$0.01 cm s^{-1}).

The reduced O_3 deposition to water and snow/ice surfaces, comparing the NUDGED and COAREG simulation results (Sect. 3.1, Tab. 1), appears to be limited in terms of relative changes in V_{d,O_3} and the total simulated O_3 deposition budget. However, these relatively small changes do substantially affect the simulated spatial distribution of surface O_3 mixing ratios over oceans and sea ice as indicated in Fig. 4. We find that the NUDGED run (Fig. 4a) systematically underestimates the mean observed surface O_3 mixing ratios for the High Arctic sites (all sites > 70 °N) by $\sim$5-10 ppb which appears to be caused by an overestimated deposition to ocean, snow and ice surfaces, also further substantiated by the following analysis of short-term variability in O_3 concentrations (Sect. 3.3). Over the Arctic sea ice and oceans the ABL is typically very shallow and atmospheric turbulence is relatively weak. This suppresses vertical mixing and entrainment of O_3 rich air from the free troposphere. Dry deposition of O_3 to the ocean or snow/ice surfaces appears to be an important removal mechanism that has a large impact on O_3 concentrations in these shallow ABLs (Clifton et al., 2020a) both in terms of magnitude but also temporal variability as we will show in Sect. 3.4. In the COAREG run, the surface O_3 mixing ratios over oceans and Arctic sea ice have increased up to 50%. Furthermore, the reduced deposition to snow/ice has also clearly affected simulated surface O_3 mixing ratios over Greenland. Most importantly, the negative bias in simulated surface O_3 mixing ratios is reduced in the COAREG run with respect to the NUDGED run (see Sect. 3.3).
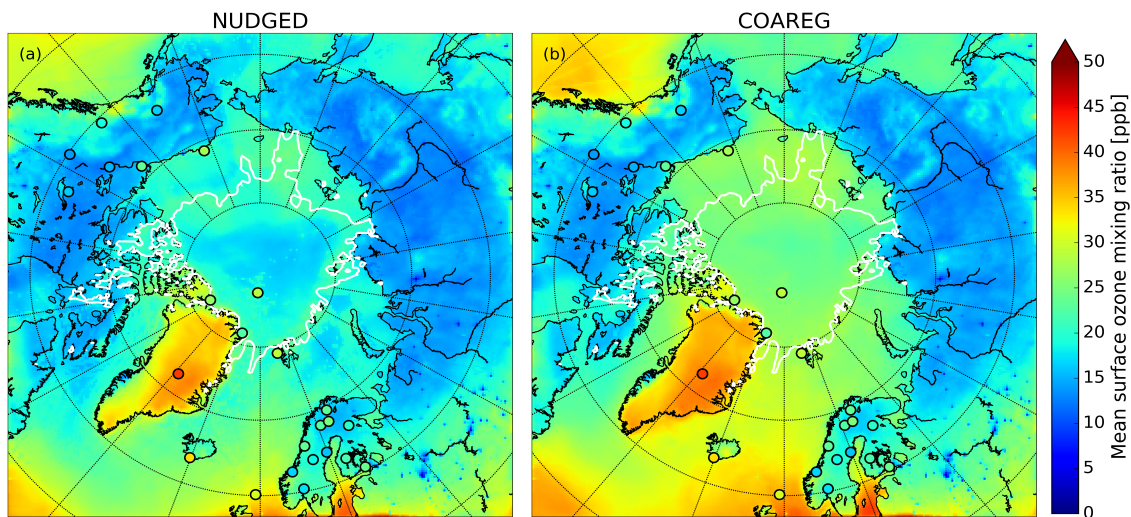
Figure 4. Spatial distribution of the simulated mean surface O$_3$ mixing ratio [ppb] for the (a) NUDGED and (b) COAREG runs. The filled circles indicate the mean observed ozone mixing ratios [ppb] for the simulated period. To indicate the sea ice extent, the white contours show the sea ice fraction of 0.5 at the start of the simulation.

3.3 Simulated and observed hourly surface ozone

In this section we show how both nudging and the application of the revised deposition scheme improves the model prediction scores of surface O$_3$ concentrations reflected in a comparison of the simulated and observed hourly surface O$_3$ mixing ratios at the three site selections (High Arctic, Remote and Terrestrial). This is according to our knowledge the first time such an oceanic O$_3$ deposition scheme coupled to a meteorology-chemistry model is evaluated against a large dataset of hourly surface O$_3$ observations. Figure 5 shows a comparison between observed and simulated hourly surface O$_3$ mixing ratios subdivided in the three site selections: High Arctic, Remote and Terrestrial. As expected, for the High Arctic sites (Fig. 5, top row) we find that the DEFAULT run is underestimating the observed surface O$_3$ mixing ratios with a mean bias of -7.7 ppb. Interestingly, nudging to ERA5 wind, temperature and humidity appears to already reduce some of the bias in the High Arctic by better representing the temporal variability in surface O$_3$. This is further examined in Sect. 3.4. However, the NUDGED run appears to still underestimate High Arctic surface O$_3$ with a bias of -3.8 ppb which is also consistent with the findings in Fig. 4, where the NUDGED run appears to underestimate surface O$_3$ mixing ratios in the High Arctic region. The COAREG run, having a reduced O$_3$ deposition sink to oceans and snow/ice appears to better represent the surface O$_3$ observations with a slight positive bias of 0.3 ppb. The MAE in the COAREG run is reduced to 4.7 ppb from 8.5 and 6.4 for the DEFAULT and NUDGED runs respectively. Furthermore, we find that the CAMS reanalysis data also underestimates surface O$_3$ in the High Arctic with a bias of -5.0 ppb and a MAE of 6.8 ppb. Note that the performance for all WRF runs and CAMS reanalysis product is varying for

315 each observational site which is further examined in Sect. 3.4.

For the Remote sites (Fig. 5, middle row), having no clear diurnal cycle in surface O_3, we find again an improvement by nudging the WRF model to ERA5 and also by including the mechanistic ocean deposition routine and reduced snow/ice deposition. This improvement appears to be most pronounced for coastal sites like Storhofdi (63.4°N,20.3°W) and Inuvik (68.4°N,133.7°W) with a reduction in the MAE of 57% and 36% respectively (not shown here). Overall, the improvement for the NUDGED and

320 COAREG runs compared to the DEFAULT run in the Remote site selection is not as significant compared to the High Arctic sites, also because of the larger role of O_3 deposition to land and vegetation, which remained unchanged in this study. We find that the CAMS data shows the best performance for the Remote sites with no bias and with a MAE of 5.6 ppb.

For the Terrestrial sites (Fig. 5, bottom row), having a clear diurnal cycle in surface O_3, all WRF runs slightly overestimate the observed surface O_3 mixing ratios with a mean bias up to 1.0 ppb. By nudging WRF to ERA5 the bias is reduced from 7.0

325 ppb to 6.0 ppb. Reducing the O_3 deposition to oceans and snow/ice increases the bias, but the MAE remains unchanged. The CAMS reanalysis data appears to perform worst for the Terrestrial sites with a bias of 6.4 ppb and a MAE of 8.0 ppb. This might be explained by the lower spatial and temporal resolution of CAMS specifically at these sites having a relatively strong diurnal cycle in ABL dynamics, O_3 deposition to vegetation and O_3 concentrations. Also a misrepresentation of emissions of precursor emissions and concentrations and the O_3 deposition to vegetation (Michou et al., 2005; Val Martin et al., 2014) might

330 explain some of the differences.

3.4 Short-term temporal variability of surface ozone in the High Arctic

In Sect. 3.3 we have shown how nudging the WRF model to ERA5 synoptic conditions and revising the O_3 deposition scheme to oceans and snow/ice can improve the model's capability to represent the observed hourly surface O_3 mixing ratios, especially for the High Arctic sites. In this section we show how the NUDGED and COAREG runs and CAMS represent the temporal

335 variation in High Arctic surface O_3 observations, focusing on a 6 out of the 25 measurement sites. These 6 High Arctic sites have been selected due to their deposition footprint being dominated by transport over, and deposition to, ocean and sea-ice covered surfaces. Figure 6 shows the observed and simulated surface O_3 time series for ASCOS, Summit, Villum, Zeppelin, Barrow and Alert. Furthermore, Tab. 2 shows the model skill indicators for the High Arctic sites. These skill indicators include the Mean Absolute Error (MAE) that represents the systematic error, the Standar Deviation of Observation minus model

340 Prediction σ_{o-p} that represents the random error and the Pearson-R correlation coefficient (R) that represents the degree of correlation.

The observations at ASCOS (Fig. 6a) show a sudden increase of surface O_3 mixing ratios from 20 to over 30 ppb around the 17th of August due to advection of relatively ozone rich air during a synoptically active period (Tjernstrom et al., 2012). Only the COAREG run appears to be able to simulate a similar increase in surface O_3 while NUDGED and CAMS show a minor

345 increase in simulated surface O_3. From the 17th of August onwards, the observations show mixing ratios between 25 and 35 ppb. The WRF simulations indicate advection of air over ocean and ice surfaces during this time period (not shown here). In the COAREG simulation, with less deposition to these surfaces, surface O_3 mixing ratios are less depleted. Only the COAREG run is able to represent these observed mixing ratios with a bias of -2.0 ppb whereas the NUDGED and CAMS are clearly

13
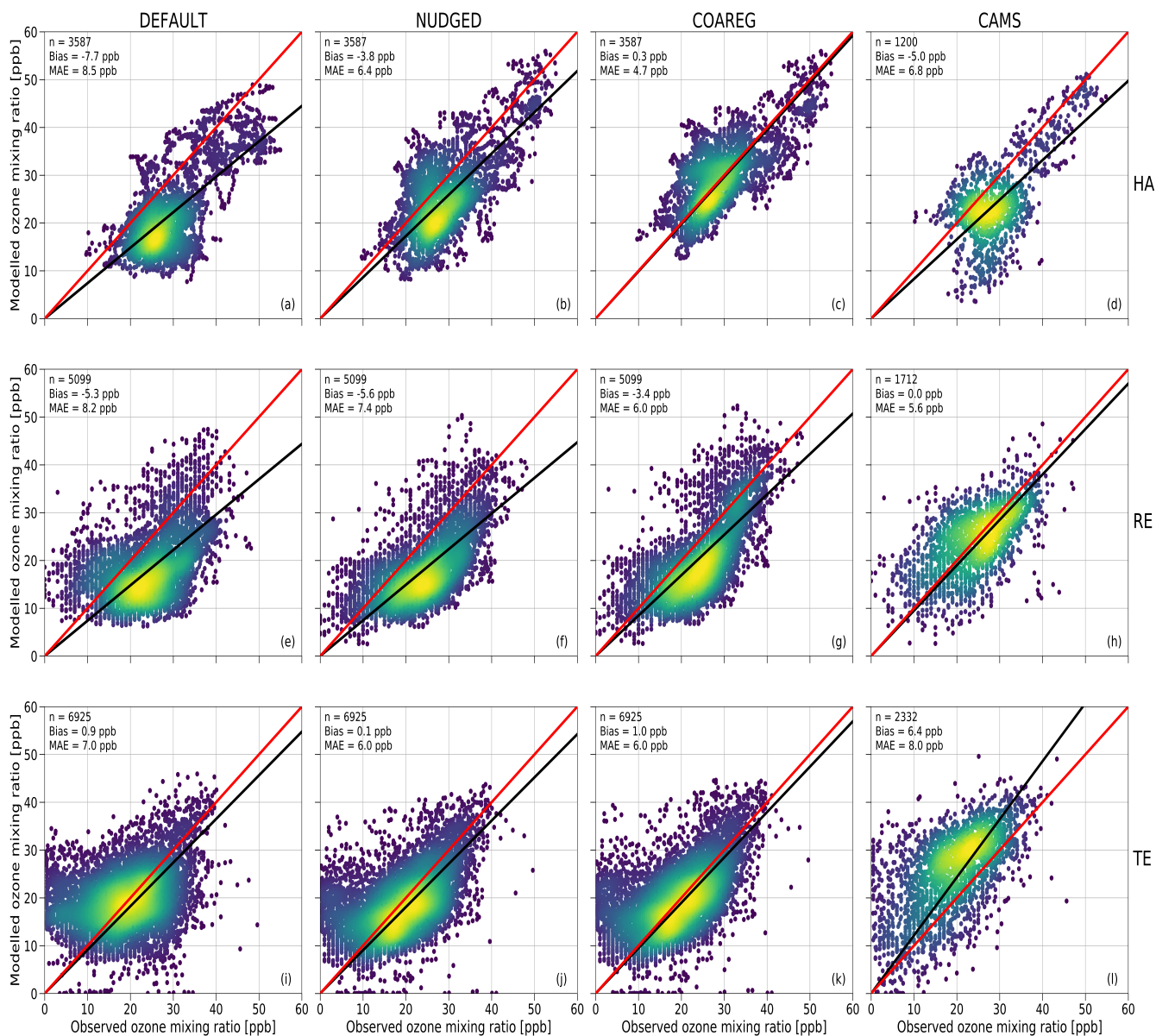
Figure 5. Comparison of the hourly observed and simulated ozone mixing ratios [ppb] for the DEFAULT (a,e,i), NUDGED (b,f,j), COAREG (c,g,k) runs and CAMS data (d,h,l) for the High Arctic (HA) (a-d), Remote (RE) (e-h) and Terrestrial (TE) (i-l) sites. The red line indicates the 1:1 line and the black line indicates the Ordinary Least Squares regression line through the origin. The number of data points (n), Bias [ppb] and Mean Absolute Error (MAE) [ppb] are shown in the top left corner. The colors represent the multivariate kernel density estimation with yellow colors having a higher density.

biased towards lower mixing ratios.

At Summit (Fig. 6b), we find a large temporal variability in observed surface O_3 between 30 and 55 ppb. From the 11th of August onwards we find a decreasing trend in observed surface O_3 down to 30 ppb before increasing to 40 ppb around the 17th of August. All models capture this specific event in terms of temporal variability even though NUDGED and COAREG are still biased at the observed minimum of 30 ppb. Furthermore, we find that the CAMS reanalysis data represents this specific period very well, also in terms of magnitude. At Summit, the increase of surface O_3 in the COAREG run relative to the NUDGED run mostly reflects the reduction of deposition to snow and ice due to the prevailing katabatic wind flow (Gorter et al., 2014). During episodes with low wind speeds the ABL becomes very stable and shallow during which deposition to snow and ice becomes an important process in removing O_3 in the ABL. In the period between the 14th and 26th of August this reduction in deposition can increase the surface O_3 mixing ratios up to 10 ppb (e.g. 23th of August). In contrast, during episodes with higher wind speeds and deeper ABLs the reduced O_3 deposition to snow hardly affects the simulated surface O_3 concentrations. Interestingly, we find that the NUDGED and COAREG simulations show a larger negative bias ($\sim$5-10 ppb) during the period with low wind speeds and shallow ABLs. Over the entire simulated period, CAMS performs best at Summit with a MAE of 3.9 ppb followed by COAREG with a MAE of 6.1 ppb.

Villum (Fig. 6c) is the only site for which the NUDGED and COAREG runs as well as the CAMS reanalysis data all systematically overestimate the observed mixing ratios, especially later into the simulation. The observations show an increase in O_3 mixing ratios from 10 to 20 ppb in the first three days of the simulation where after it remains between 20 and 30 ppb with relatively low temporal variability compared to some of the other sites (e.g. Summit, Barrow). Both the NUDGED and COAREG runs simulate mixing ratios up to 40 ppb and CAMS simulates maximum surface O_3 mixing ratios of 35 ppb. In terms of representing the magnitude of surface O_3 mixing ratios CAMS performs best with a MAE of 4.5.

Zeppelin (Fig. 6d) and Barrow (Fig. 6e) show similar behaviour in terms of observation-model comparison. For both locations the CAMS reanalysis data systematically underestimates observed ozone mixing ratios with a biases > 10 ppb. In the NUDGED run the bias equals -6.9 and -4.6 ppb for Zeppelin and Barrow, respectively. In the COAREG run the bias is reduced to -1.0 and -0.2 ppb for Zeppelin and Barrow respectively. This reduction in bias is, together with ASCOS, the largest among the 6 High Arctic sites and shows the large sensitivity to the representation of O_3 deposition. At Barrow, the dominant wind directions during the simulation period are NW-NE giving a footprint mostly from the Arctic sea ice and ocean. Especially in the period from the 23th of August onward the COAREG run is very accurate in representing the magnitude as well as the temporal variability in observed surface O_3. During this period, the NUDGED run simulates surface O_3 mixing ratios up to 5 ppb lower due to the overestimated deposition to oceans and sea ice. At both sites, the model performance of COAREG is in the same order of magnitude with an MAE, $\sigma_{\text{o-p}}$ and R of $\sim$ 3.5 ppb, 4.2 ppb and 0.65 respectively.

At Alert (Fig. 6f), we find a relatively steady increase in observed surface O_3 from 20 ppb at the start of the simulation to 30 ppb at the end of the simulation. The temporal variability, both in observed and simulated surface O_3 appears to be lower compared to some of the other High Arctic sites. Again, the statistical parameters such as MAE, $\sigma_{\text{o-p}}$ and R improve in the COAREG run with respect to the NUDGED run. At Alert, we find that CAMS has the lowest MAE and $\sigma_{\text{o-p}}$ of 3.0 ppb and 3.4 ppb respectively.

The model performance in terms of temporal variability in surface O_3 observations is diagnosed by using the Pearson-R correlation coefficient. The model performance improved for all six sites in the COAREG run with respect to the NUDGED run. The COAREG run includes temporal variability in O_3 deposition due to variability in waterside turbulent transport which can explain additional improvements in representing the temporal variability of surface O_3. The COAREG simulation performs best for 5 out of the 6 observational sites in terms of Pearson-R correlation coefficient and is only outperformed by CAMS at Summit. Overall, we find that coupling the WRF model to the mechanistic COAREG ocean-atmosphere exchange representation decreases the MAE and $\sigma_{\text{o-p}}$ for all High Arctic sites except for Villum by better representing the magnitude of, but also temporal variability in observed surface O_3. The CAMS reanalysis data is performing well for some locations (e.g. Summit, Alert) while for Zeppelin and Barrow the discrepancy is among the largest we found in the observation-model comparison.

Table 2. MAE [ppb], $\sigma_{\text{o-p}}$ [ppb] and Pearson-R correlation coefficient (R) [-] for the NUDGED and COAREG runs and CAMS reanalysis data at the ASCOS, Summit, Villum, Zeppelin, Barrow and Alert observational sites. The lowest model error and highest correlation have been made bold for every site.

	ASCOS			Summit			Villum			Zeppelin			Barrow			Alert		
	MAE	$\sigma_{\text{o-p}}$	R	MAE	$\sigma_{\text{o-p}}$	R	MAE	$\sigma_{\text{o-p}}$	R	MAE	$\sigma_{\text{o-p}}$	R	MAE	$\sigma_{\text{o-p}}$	R	MAE	$\sigma_{\text{o-p}}$	R
NUDGED	9.4	4.3	0.46	7.5	7.0	0.62	5.4	5.7	0.46	7.4	4.8	0.62	5.5	4.6	0.49	4.4	5.1	0.68
COAREG	**3.1**	**3.2**	**0.67**	6.1	5.8	0.67	7.8	**4.5**	0.6	**3.6**	**4.3**	**0.69**	**3.4**	**4.2**	0.6	3.6	4.3	**0.74**
CAMS	7.5	4.5	0.07	**3.9**	**4.3**	**0.78**	**4.5**	**4.5**	0.38	11.1	5.3	0.4	11.1	4.9	0.56	**3.0**	**3.4**	0.65

4 Discussion

This study demonstrates the impact of a mechanistic representation of ocean-atmosphere O_3 exchange to simulate the magnitude and temporal variability of hourly surface O_3 concentrations in the Arctic. We show that the modelled sensitivity of the surface O_3 concentrations to the representation of O_3 to ocean, ice and snow surfaces is high, even though the total deposition budget is an order of magnitude smaller than the deposition to land and vegetation. Using a mechanistic oceanic O_3 deposition representation and reduced O_3 deposition to snow and ice greatly reduced the negative bias in surface O_3, especially in the high Arctic. Furthermore, the short-term temporal variability in surface O_3 was also better represented by the mechanistic representation of oceanic O_3 deposition by also accounting for temporal variations in the driving processes of oceanic O_3 deposition such as waterside turbulent transport.

Our main objective was to address the impact of a mechanistic oceanic O_3 deposition representation, including spatial and temporal variability, on the magnitude and temporal variability of surface O_3 concentrations and to evaluate this with a large dataset of 25 observational sites in and around the Arctic. We show that Arctic surface O_3 concentrations are sensitive to the representation of O_3 deposition to oceans and sea-ice especially at coastal sites and sites with latitudes >70°N. At sites with a more terrestrial footprint (e.g. Norway, Sweden, Finland), the comparison of modelled and observed surface O_3 concentrations also shows a discrepancy. As expected, this discrepancy has not been resolved introducing the more mechanistic representation
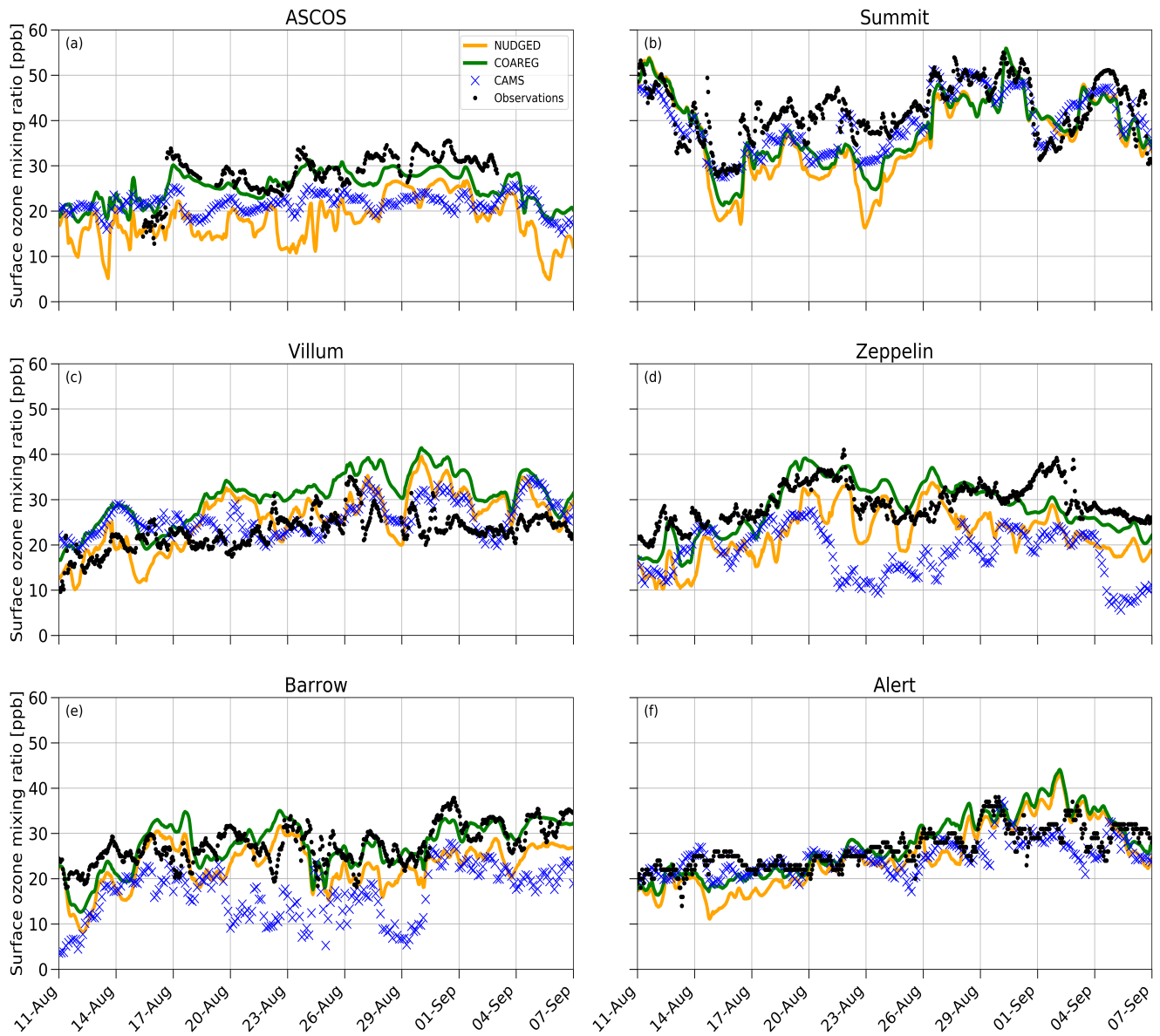
Figure 6. Temporal evolution of hourly surface O$_3$ mixing ratios [ppb] for the NUDGED (yellow) and COAREG (green) runs, CAMS data (blue crosses) and observations (black dots) at ASCOS ($\sim$87.4°N,$\sim$6.0°W), Summit (72.6°N,38.5°W), Villum (81.6°N,16.7°W), Zeppelin (78.9°N,11.9°E), Barrow (71.3°N,156.6°W) and Alert (82.5°N,62.3°W).

of O_3 deposition oceans and modified snow/sea-ice deposition rate. In terms of deposition, these sites are mostly influenced by O_3 deposition to vegetation and land (e.g. Silva and Heald, 2018; Wong et al., 2019; Clifton et al., 2020b). In the WRF simulations, dry deposition of O_3 to vegetation (mostly land-use class: 'wooded tundra') amounts to $\sim$0.2-1.0 cm s^{-1} with a clear diurnal cycle. Dry deposition of O_3 to 'bare tundra' is in the order of 0.1-0.15 cm s^{-1} which is slightly higher than observed by Van Dam et al. (2015). A detailed analysis of O_3 deposition to land and vegetation is beyond the scope of this study and would require a different strategy, e.g. direct comparison with O_3 flux measurements (e.g. Van Dam et al., 2016). However, a better understanding and model representation of the drivers of O_3 deposition to vegetation and land, including the diurnal and seasonal variability of these drivers (Lin et al., 2019), is anticipated to also result in a better representation of short-term variability of surface O_3 over land.

The COAREG scheme has been developed and validated against eddy-covariance measurements over mostly (sub-)tropical waters (Bariteau et al., 2010; Helmig et al., 2012). The COAREG routine has been applied to study the effects of wind speed and sea state on ocean atmosphere gas transfer (Blomquist et al., 2017; Bell et al., 2017; Porter et al., 2020). We do expect that these main drivers, being waterside turbulent transfer and chemical enhancement with dissolved iodide, also controls oceanic O_3 deposition at high latitudes. Indirect evaluation of oceanic O_3 deposition through comparison of surface O_3 observations instead of direct oceanic O_3 flux measurements indicates that including this mechanistic representation of O_3 deposition improves both the modelled magnitude and temporal variability in surface O_3 observations. However, a lack of oceanic O_3 deposition flux measurements hampers the direct model evaluation of the high-latitude O_3 deposition flux. This is expected to be soon resolved by getting access to O_3 flux observations collected in the Multidisciplinary drifting Observatory for the Study of Arctic Climate (MOSAiC) 1-year field campaign.

Furthermore, we have reduced the deposition to snow and ice following Helmig et al. (2007a) and (Clifton et al., 2020b). Results of Helmig et al. (2007a) also motivated follow-up observational and modelling studies aiming at the development of more mechanistic representations of O_3 deposition to snow/ice covered surfaces. For example, efforts have been made to simulate O_3 dynamics in and above the snowpack using a 1D model setup to explain observations of O_3 and NO_x concentrations measured above and inside the Summit snowpack (Van Dam et al., 2015). This 1D modelling study showed the main role of aqueous-phase oxidation of O_3 with formic acid in the snowpack (Murray et al., 2015). Comparable 1D modelling studies focused on assessing the role of catalytic ozone loss via bromine radical chemistry in the snowpack interstitial air (Thomas et al., 2011; Toyota et al., 2014). However, these studies mainly addressed the role of some of this snowpack chemistry in explaining, partly observed, O_3 concentrations and not so much on snow-atmosphere O_3 fluxes and derived deposition rates that would corroborate the inferred very small O_3 deposition rates by Helmig et al. (2007a). Clifton et al. (2020b) summarized that accurate process-based modelling of O_3 deposition to snow requires better understanding of the underlying processes and dependencies. An eddy-covariance system has been set up as part of the MOSAiC campaign and will provide year-round O_3 deposition fluxes to several land surface types such as open ocean and sea ice with fluctuating snow cover. These measurements will further enhance our understanding of O_3 deposition in shallow ABLs at high latitudes (Clifton et al., 2020a) and the further role in regional atmospheric chemistry.

In this study we used the COAREG transfer algorithm version 3.6 which is extended with a two-layer scheme for surface

resistance compared to the previous versions (Fairall et al., 2007, 2011) and similar to Luhar et al. (2018). Our WRF simulations excluded the additional role of chlorophyll, Dissolved Organic Matter (DOM) or other species such as DMS on chemical enhancement of O_3 in surface waters. Experimental studies have shown that DMS, chlorophyll, or other reactive organics, may enhance the removal of O_3 at the sea surface (Chang et al., 2004; Clifford et al., 2008; Reeser et al., 2009; Martino et al., 2012). The global modelling study by Ganzeveld et al. (2009) included a chlorophyll-O_3 reactivity that increased linearly with chlorophyll concentration as a proxy for the role of DOM in oceanic O_3 deposition. Including this reaction substantially enhances O_3 deposition to coastal waters such that actually observed O_3 deposition to these coastal waters is well reproduced (Ganzeveld et al., 2009). Other studies such as Luhar et al. (2017); Pound et al. (2019) ignored the potential role of DOM-O_3 chemistry in oceanic O_3 deposition. Luhar et al. (2018), which did not explicitly consider coastal waters, even suggested that including such a reaction deteriorates the comparison with O_3 flux observations above open oceans. A considerable uncertainty in the DOM-O_3 reaction is the second-order rate coefficient but also the magnitude and variability in oceanic DOM concentrations (Luhar et al., 2018). To test the sensitivity of our model setup to other reactants in the surface water we have performed an additional sensitivity analysis including the chlorophyll-O_3 and DMS-O_3 reactions from Ganzeveld et al. (2009). Oceanic chlorophyll concentrations have been retrieved from the 9×9 km resolution MODIS chlorophyll-α dataset available at https://modis.gsfc.nasa.gov/data/dataprod/chlor_a.php (last access: 14 Aug 2020). Chlorophyll-α concentrations are typically < 3 mg m^{-3} for open oceans up to 25 mg m^{-3} for coastal waters. For oceanic DMS concentrations, we use the monthly climatology from Lana et al. (2011). The sensitivity study with chlorophyll as extra reactant indicated a slight increase (up to 5%) in deposition to coastal waters with chlorophyll concentrations up to 25 mg m^{-3}. However, the resulting effect on surface O_3 concentrations was not significant due to the large fraction of oceans with very low (< 3 mg m^{-3}) chlorophyll-α concentrations. Also the reactions with oceanic DMS appear to be weak due to relatively low DMS concentrations in August/September. These sensitivity studies indicate that Γ_{aq} is the main driver of chemical reactivity of O_3 in the Arctic ocean in summer. However a potential sensitivity of these reactants on Arctic O_3 deposition could especially be expected in the spring to summer transition following from algal blooms (Stefels et al., 2007; Riedel et al., 2008). However, in springtime the removal of Arctic O_3 near the surface is also largely affected by halogen chemistry (Pratt et al., 2013; Thomas et al., 2013; Yang et al., 2020) and which is known to explain observed surface O_3 mixing ratios dropping to 0 ppb (Halfacre et al., 2014). However, this feature is of less relevance for the presented study with the evaluation being focused on August/September and when the role of halogen chemistry is deemed being less important (Yang et al., 2020).

We nudged the WRF model to the ECMWF ERA5 reanalysis product to ensure a fair model evaluation with observations due to a better representation of the synoptic conditions. This indicated the important role of the model representation of meteorology, e.g. advection of polluted air and mixing/entrainment of O_3 in the ABL, in representing the observed surface O_3 concentrations. The model evaluation was set up at a resolution of 30×30 km which is in the order of the ERA5 reanalysis data ($0.25°\times0.25°$) used for initial conditions, boundary conditions and nudging. Here, we opted for a 30 km grid spacing because we expect that the main drivers of tropospheric O_3 (chemical production and destruction, stratosphere-troposphere transport, dry deposition and mixing/advection processes) can be sufficiently resolved at this grid spacing especially over the relatively homogeneous ocean, ice and snow surfaces. However, we do realize that such a coarse grid spacing may have hampered representing local

air flow phenomena such as katabatic winds (Klein et al., 2001) which could explain some of the mismatch at sites like Villum (Nguyen et al., 2016). Another justification for the 30 km grid spacing was to limit computational time and to have a large enough domain to cover the entire region above 60 °N to conduct a large pan-Arctic evaluation while at the same time having all observational sites far enough from the domain boundaries to limit the effect of the imposed meteorological and chemical boundary conditions.

In general, the relatively scarce Arctic observations introduces constraints to modelling studies and limits the potential of these results to be extrapolated to other seasons and lower latitudes. In this case, this includes the uncertainty in the magnitude and distribution of driving factors of oceanic O_3 deposition such as I^-_{aq} (Sherwen et al., 2019) or DOM. New I^-_{aq} measurements at high latitudes, for example those performed during the year-round MOSAiC expedition, will be very useful to better constrain the global I^-_{aq} distributions as well as mechanistic oceanic O_3 deposition representations. Measurements of O_3 concentrations and deposition fluxes to the Arctic ocean can assist to better constrain these modelling setups in terms of magnitude and temporal variability and potentially indicate of the sensitivity to other environmental factors such as wind speed in waters with low reactivity. Furthermore, including the role of halogen chemistry (Pratt et al., 2013; Thompson et al., 2017) might give an indication of the combined role of halogens and oceanic deposition in removing O_3 and explaining the magnitude and short- but also long-term variability of O_3 concentrations in the High Arctic.

5 Conclusions

The mesoscale meteorology-chemistry model Polar-WRF-Chem was coupled to the Coupled Ocean-Atmosphere Response Experiment Gas transfer algorithm (COAREG) to allow for a mechanistic representation of ocean-atmosphere exchange of O_3. This scheme represents effects of molecular diffusion, solubility, waterside turbulent transfer and chemical enhancement of O_3 uptake through its reactions with dissolved iodide. The GOAREG scheme replaces the constant surface uptake resistance approach often applied in ACTMs. Furthermore, we have increased the modelled O_3 surface uptake resistance to snow and ice. In total, three simulations were performed: 1) default WRF setup (DEFAULT), 2) nudged to ERA5 synoptic conditions (NUDGED) and 3) with adjustments to O_3 surface uptake resistance as described above (COAREG). Furthermore, the CAMS global reanalysis data product has also been included in the presented evaluation on High Arctic surface O_3. This CAMS product is widely used in air quality assessments and to constrain regional scale modelling experiments. This provides additional information on the quality of the CAMS data products but also on potential issues in the representation of O_3 sources and sinks, e.g., oceanic and snow/sea-ice deposition, for the High Arctic. The modelling approach was set up for one month at the end-of-summer 2008 and evaluated against hourly surface O_3 at 25 sites for latitudes > 60°N including observations over the Arctic sea ice as part of the ASCOS campaign.

Using the mechanistic representation of ocean-atmosphere exchange, O_3 deposition velocities were simulated in the order of 0.01 cm s^{-1} compared to ~0.05 cm s^{-1} in the constant surface uptake resistance approach. In the COAREG run, the spatial variability (0.01 to 0.018 cm s^{-1}) in the mean O_3 deposition velocities expressed the sensitivity to chemical enhancement with dissolved iodide. The temporal variability of O_3 deposition velocities (up to ±20% around the mean) is governed by surface

wind speeds and expressed differences in waterside turbulent transport. In the constant surface uptake resistance approach, there is no spatial variability in O_3 deposition velocities and the temporal variability is determined by the aerodynamic resistance term that can be significant at low wind speeds. Using the mechanistic representation of ocean-atmosphere exchange reduced the total simulated O_3 deposition budget to water bodies by a factor of 3.3 compared to the default constant ocean uptake rate approach and the increase in surface uptake resistance to snow and ice reduced the deposition budget by a factor of 2.4.

Despite the fact that O_3 deposition to oceans, snow and ice surfaces only constitutes a small term in the total O_3 deposition budget (> 90% of the deposition is to land), we find a substantial sensitivity to the simulated surface O_3 mixing ratios. In the COAREG run, the simulated mean monthly surface O_3 mixing ratios have increased up to 50% in the typically shallow Arctic ABL above the oceans and sea-ice relative to the NUDGED run. The mechanistic representation of O_3 deposition to oceans, but also nudging to ERA5 synoptic conditions, resulted in a substantial improved representation of surface O_3 observations, especially for the High Arctic sites having latitudes > 70 °N. The DEFAULT run underestimated the observed surface O_3 mixing ratios with a bias of -7.7 ppb whereas the NUDGED and COAREG runs had a bias of -3.8 ppb and 0.3 ppb, respectively. The evaluation of the WRF runs at individual High Arctic sites showed that using the mechanistic representation of O_3 deposition to oceans and nudging the model to ERA5 better represents the surface O_3 observations in terms of magnitude as well as short-term temporal variability. Similar to the NUDGED run, CAMS underestimated High Arctic observed surface O_3 with a bias of -5.0 ppb indicating that for this product the deposition removal mechanism to oceans and snow/ice might also be overestimated and should be reconsidered.

This study highlights the impact of a mechanistic representation of oceanic O_3 deposition on Arctic surface O_3 concentrations at a high (hourly) temporal resolution. It mostly corroborates the findings of global scale studies (e.g. Ganzeveld et al., 2009; Luhar et al., 2017; Pound et al., 2019) and recommends that the representation of O_3 deposition to oceans and snow/ice in global and regional scale ACTMs should be revised. This revision is needed not only to better quantify the O_3 budget at the global scale, but also to better represent the observed magnitude and short-term temporal variability of surface O_3 at the regional scale. In addition, explicit consideration of the mechanisms involved in O_3 removal by the oceans (and sea-ice/snow pack) are essential to also evaluate the role of potentially important feedback mechanisms and future trends in- and the role of O_3 in Arctic climate change as a function of declining sea ice cover, increasing emissions and changes in oceanic biogeochemical conditions. On the regional scale, this study also has implications for methods to quantify future trends in Arctic tropospheric O_3, Arctic air pollution and climate in a period of declining sea ice and increasing local emissions of precursors.

Appendix A: WRF physical and chemical parameterization schemes.

Table A1. WRF physical and chemical parameterization schemes.

WRF option	Configuration
Physical parameterizations	
Microphysics	WSM5 (Hong et al., 2004)
Long wave radiation	RRTMG (Iacono et al., 2008)
Short wave radiation	RRTMG (Iacono et al., 2008)
Surface layer	Monin-Obukhov (Janjić, 2001)
Land surface	Noah (Chen and Dudhia, 2001)
Boundary layer	MYJ (Janjić, 1994)
Cumulus	Kain-Fritsch (Kain, 2004)
Chemistry	
Gas-phase	CBM-Z (Gery et al., 1989; Zaveri and Peters, 1999)
Photolysis	Fast-J (Wild et al., 2000)
Emissions	
Anthropogenic	EDGAR (Janssens-Maenhout et al., 2017)
Biogenic	MEGAN (Guenther et al., 2012)
Boundary conditions	
Meteorology	ERA5 ($0.25^\circ \times 0.25^\circ$) (Hersbach et al., 2020)
Chemistry	CAMS ($0.75^\circ \times 0.75^\circ$) (Inness et al., 2019)

Appendix B: Formulation of the air- and waterside resistance terms

The exchange velocity, in this case deposition, of ozone (V_{d,O_3}) [m s^{-1}] is calculated from the waterside resistance (r_w) [s m^{-1}] and air side resistance terms ($r_a + r_a$) [s m^{-1}] as follows:

$$V_{d,O_3} = \frac{1}{\alpha r_w + r_a + r_b}. \tag{B1}$$

Here, α [-] is the dimensionless solubility of O$_3$ in sea water calculated from SST [K] following Morris (1988) as

$$\alpha = 10^{-0.25 - 0.013(SST - 273.16)} \tag{B2}$$

and the waterside resistance term (r_w) is calculated as

$$r_w = \sqrt{a * D} \frac{\Psi K_1(\xi_\delta) \cosh \lambda + K_0(\xi_\delta) \sinh \lambda}{\Psi K_1(\xi_\delta) \sinh \lambda + K_0(\xi_\delta) \cosh \lambda}. \tag{B3}$$

Here, a [s^{-1}] is the chemical reactivity of O$_3$ with I$^-_{aq}$ calculated with the second order rate coefficient [M^{-1} s^{-1}] from Magi et al. (1997) and the I$^-_{aq}$ concentrations [M] from Sherwen et al. (2019):

$$a = k \cdot [I^-_{aq}] = \exp(\frac{-8772.2}{SST} + 51.5) \cdot [I^-_{aq}]. \tag{B4}$$

In Eq. B3, D [m^2 s^{-1}] is the molecular diffusivity of O$_3$ in ocean water and is calculated from the kinematic viscosity ν [m^2 s^{-1}] and the waterside Schmidt number (S_{cw}) [-] as

$$D = \frac{\nu}{S_{cw}} = \frac{\mu}{\rho} / [\sqrt{44/48} \cdot \exp(-0.055 \cdot SST + 22.63)] \tag{B5}$$

where μ [kg m^{-1} s^{-1}] is the dynamic viscosity of seawater and ρ [kg m^{-3}] is the density of seawater.

Finally, the air side resistance terms ($r_a + r_b$) [s m^{-1}] of the deposition velocity in Eq. B1 are calculated as

$$r_a + r_b = [C_d^{-1/2} + 13.3 S_c^{1/2} - 5 + \frac{\log(S_c)}{2\kappa}] / u_{*,a} \tag{B6}$$

where C_d [-] is the momentum drag coefficient, S_{ca} [-] is the Schmidt number for ozone in the atmosphere, κ is the Von Karman constant (0.4) and $u_{*,a}$ [m s^{-1}] is the friction velocity in the atmosphere. The $r_a + r_b$ term is typically in the order of 100 s m^{-1} (Fairall et al., 2011).

Compared to COAREG version 3.1 (Fairall et al., 2007, 2011), COAREGv3.6 is extended with a two-layer scheme based on Luhar et al. (2018). This extension is included in the second term of the waterside resistance term (Eq. B3). Here, $\Psi = \sqrt{1 + (\kappa u_{*,w} \delta_m / D)}$, $\xi_\delta = \sqrt{2 a b (\delta_m + b D/2)}$, and $\lambda = \delta_m \sqrt{a/D}$ with $b = 2/(\kappa u_{*,w})$. This part of the equation is a function of the chemical reactivity a [s^{-1}] (Eq. B4), the waterside friction velocity $u_{*,w}$ [m s^{-1}], the molecular diffusivity of O$_3$ in ocean water (Eq. B5) and δ_m [m] representing the depth of the interface between the top water layer and the underlying turbulent layer. In this study we have applied $\delta_m = c_0 \sqrt{D/a}$ with $c_0 = 0.4$ based on Luhar et al. (2018). $K_0(\xi_\delta)$ and $K_1(\xi_\delta)$ are the modified Bessel functions of the second kind of order 0 and 1, respectively. For more information on the derivation of the formulas please visit Fairall et al. (2007, 2011); Luhar et al. (2018).

Figure B1 shows the sensitivity of the COAREG routine coupled to WRF to the environmental factors wind speed, SST and
Iodide concentration. The sensitivity to wind speeds (Fig. B1a) expresses the role of waterside turbulent transport and aerody-

580   namic resistance. For low wind speeds waterside turbulent transport is limited and therefore limits the exchange of O_3 from
the atmosphere to the ocean. At high wind speeds, the dry deposition of O_3 is limited by chemical reactivity of O_3 with I^-_{aq}
at typical Arctic SSTs of 5 °C and I^-_{aq} concentrations of 60 nM (see also Fig. C1). At very low wind speeds (< 3 m s^{-1}) the
aerodynamic resistance poses an extra restriction on the ocean-atmosphere exchange of O_3. The sensitivity to SST (Fig. B1b)
mostly represents the role of solubility (Eq. B2) with warmer waters having a lower solubility. In contrast to Luhar et al. (2018),

585   the SST is not used to calculate the I^-_{aq} concentrations and does therefore not show a positive correlation. The sensitivity to I^-_{aq}
(Fig. B1c) represents the role of chemical enhancement which is stronger than the generally compensating effect of solubility
in warmer waters for typical Arctic conditions.
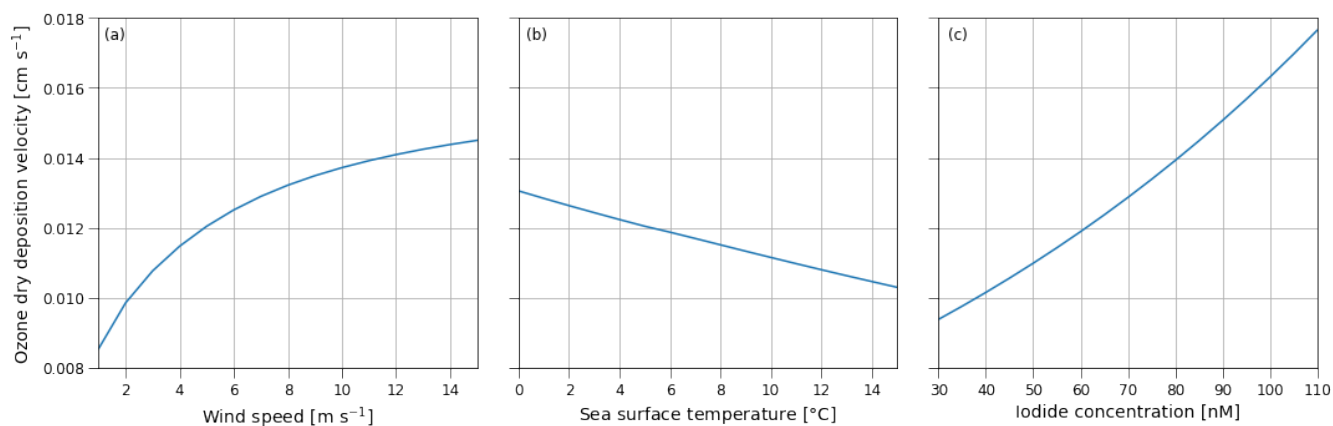
Figure B1. Sensitivity of the ozone dry deposition velocity from COAREG to the environmental factors 10-meter wind speed [m s^{-1}] (a),
sea surface temperature [°C] (b) and sea surface Iodide concentration [nM] (c) using typical values of 10-meter wind speed, sea surface
temperature and Iodide concentration of 5 m s^{-1}, 5 °C and 60 nM respectively. Note that the sensitivity to sea surface temperature does not
include effects of increasing reactivity but mostly represents the effect of reduced solubility (Eq. B2).

Appendix C: Spatial distribution of oceanic Iodide
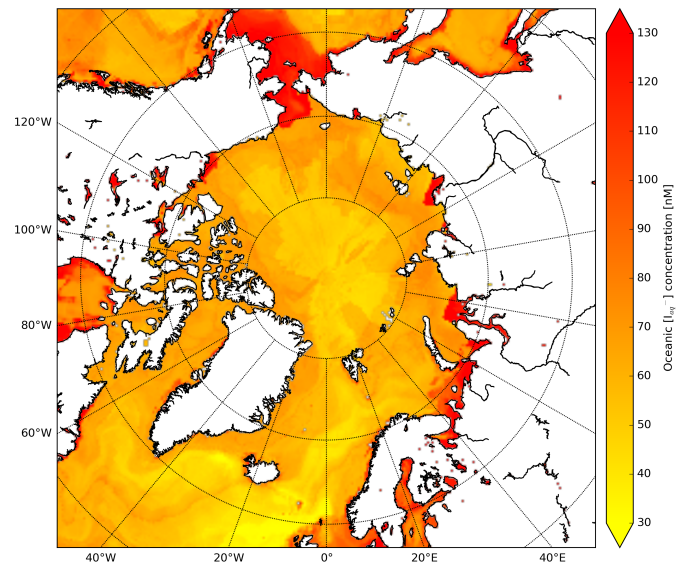
Figure C1. Spatial distribution of Sherwen et al. (2019) oceanic Iodide concentrations [nM] at the start of the simulation.

Appendix D: Surface ozone measurement sites.

Table D1. Surface ozone measurement sites subdivided in the 'High Arctic', 'Remote' and 'Terrestrial' site selections.

Name	Abbreviation	Group	Latitude [°N]	Longitude [°E]
Alert	ALT	High Arctic	82.5	-62.3
ASCOS	ASC	High Arctic	$\sim$ 87.4	$\sim$ -6.0
Barrow	BRW	High Arctic	71.3	-156.6
Zeppelin	NYA	High Arctic	78.9	11.9
Summit	SUM	High Arctic	72.6	-38.5
Villum	VIL	High Arctic	81.6	-16.7
Denali NP	DEN	Remote	63.7	-149.0
Esrange	ESR	Remote	67.9	21.1
Karasjok	KAS	Remote	69.5	25.2
Inuvik	INU	Remote	68.4	-133.7
Lerwick	SIS	Remote	60.1	-1.2
Pallas	PAL	Remote	68.0	21.1
Storhofdi	ICE	Remote	63.4	-20.3
Yellowknife	YEL	Remote	62.5	-114.4
Ahtari	AHT	Terrestrial	62.6	24.2
Bredkalen	BRE	Terrestrial	63.9	15.3
Fort Liard	FOR	Terrestrial	60.2	-123.5
Hurdal	HUR	Terrestrial	60.4	11.1
Karvatn	KRV	Terrestrial	62.8	8.9
Norman Wells	NOR	Terrestrial	65.3	-123.8
Oulanka	OUX	Terrestrial	66.3	29.4
Tustervatn	TUV	Terrestrial	65.8	13.9
Vindeln	VDI	Terrestrial	64.3	19.8
Virolahti	VIR	Terrestrial	60.5	27.7
Whitehorse	WHI	Terrestrial	60.7	-135.0

References

Ainsworth, E. A., Yendrek, C. R., Sitch, S., Collins, W. J., and Emberson, L. D.: The effects of tropospheric ozone on net primary productivity and implications for climate change, Annual review of plant biology, 63, 637–661, 2012.

Arnold, S. R., Law, K. S., Brock, C. A., Thomas, J. L., Starkweather, S. M., von Salzen, K., Stohl, A., Sharma, S., Lund, M. T., Flanner, M. G., et al.: Arctic air pollution: Challenges and opportunities for the next decade, Elementa: Science of the Anthropocene, 2016.

Bariteau, L., Helmig, D., Fairall, C., Hare, J., Hueber, J., and Lang, E.: Determination of oceanic ozone deposition by ship-borne eddy covariance flux measurements, Atmospheric Measurement Techniques, 3, 441–455, 2010.

Bell, T. G., Landwehr, S., Miller, S. D., De Bruyn, W. J., Callaghan, A. H., Scanlon, B., Ward, B., Yang, M., and Saltzman, E. S.: Estimation of bubble-mediated air-sea gas exchange from concurrent DMS and CO2 transfer velocities at intermediate-high wind speeds, Atmospheric Chemistry and Physics, 17, 9019–9033, 2017.

Blomquist, B., Brumer, S., Fairall, C., Huebert, B., Zappa, C., Brooks, I., Yang, M., Bariteau, L., Prytherch, J., Hare, J., et al.: Wind speed and sea state dependencies of air-sea gas transfer: Results from the high wind speed gas exchange study (HiWinGS), Journal of Geophysical Research: Oceans, 122, 8034–8062, 2017.

Bromwich, D. H., Otieno, F. O., Hines, K. M., Manning, K. W., and Shilo, E.: Comprehensive evaluation of polar weather research and forecasting model performance in the Antarctic, Journal of Geophysical Research: Atmospheres, 118, 274–292, 2013.

Chance, R., Baker, A. R., Carpenter, L., and Jickells, T. D.: The distribution of iodide at the sea surface, Environmental Science: Processes & Impacts, 16, 1841–1859, 2014.

Chang, W., Heikes, B. G., and Lee, M.: Ozone deposition to the sea surface: chemical enhancement and wind speed dependence, Atmospheric Environment, 38, 1053–1059, 2004.

Chen, F. and Dudhia, J.: Coupling an advanced land surface–hydrology model with the Penn State–NCAR MM5 modeling system. Part I: Model implementation and sensitivity, Monthly weather review, 129, 569–585, 2001.

Chen, X., Quéléver, L. L., Fung, P. L., Kesti, J., Rissanen, M. P., Bäck, J., Keronen, P., Junninen, H., Petäjä, T., Kerminen, V.-M., et al.: Observations of ozone depletion events in a Finnish boreal forest, Atmospheric Chemistry and Physics, 18, 49–63, 2018.

Clifford, D., Donaldson, D., Brigante, M., D'Anna, B., and George, C.: Reactive uptake of ozone by chlorophyll at aqueous surfaces, Environmental science & technology, 42, 1138–1143, 2008.

Clifton, O., Paulot, F., Fiore, A., Horowitz, L., Correa, G., Baublitz, C., Fares, S., Goded, I., Goldstein, A., Gruening, C., et al.: Influence of dynamic ozone dry deposition on ozone pollution, Journal of Geophysical Research: Atmospheres, 125, e2020JD032 398, 2020a.

Clifton, O. E., Fiore, A. M., Massman, W. J., Baublitz, C. B., Coyle, M., Emberson, L., Fares, S., Farmer, D. K., Gentine, P., Gerosa, G., et al.: Dry deposition of ozone over land: processes, measurement, and modeling, Reviews of Geophysics, 58, e2019RG000 670, 2020b.

Cooper, O. R., Parrish, D., Ziemke, J., Cupeiro, M., Galbally, I., Gilge, S., Horowitz, L., Jensen, N., Lamarque, J.-F., Naik, V., et al.: Global distribution and trends of tropospheric ozone: An observation-based review, 2014.

Cooper, O. R., Schultz, M. G., Schröder, S., Chang, K.-L., Gaudel, A., Benítez, G. C., Cuevas, E., Fröhlich, M., Galbally, I. E., Molloy, S., et al.: Multi-decadal surface ozone trends at globally distributed remote locations, Elementa: Science of the Anthropocene, 8, 2020.

Fairall, C., Helmig, D., Ganzeveld, L., and Hare, J.: Water-side turbulence enhancement of ozone deposition to the ocean, Atmospheric Chemistry and Physics, 2007, 443–451, 2007.

625   Fairall, C., Yang, M., Bariteau, L., Edson, J., Helmig, D., McGillis, W., Pezoa, S., Hare, J., Huebert, B., and Blomquist, B.: Implementation of the Coupled Ocean-Atmosphere Response Experiment flux algorithm with CO2, dimethyl sulfide, and O3, Journal of Geophysical Research: Oceans, 116, 2011.

Fairall, C. W., Bradley, E. F., Rogers, D. P., Edson, J. B., and Young, G. S.: Bulk parameterization of air-sea fluxes for tropical ocean-global atmosphere coupled-ocean atmosphere response experiment, Journal of Geophysical Research: Oceans, 101, 3747–3764, 1996.

630   Fan, S.-M., Wofsy, S. C., Bakwin, P. S., Jacob, D. J., and Fitzjarrald, D. R.: Atmosphere-biosphere exchange of CO2 and O3 in the central Amazon forest, Journal of Geophysical Research: Atmospheres, 95, 16 851–16 864, 1990.

Gallagher, M., Beswick, K., and Coe, H.: Ozone deposition to coastal waters, Quarterly Journal of the Royal Meteorological Society, 127, 539–558, 2001.

Ganzeveld, L., Helmig, D., Fairall, C., Hare, J., and Pozzer, A.: Atmosphere-ocean ozone exchange: A global modeling study of biogeo-
635   chemical, atmospheric, and waterside turbulence dependencies, Global Biogeochemical Cycles, 23, 2009.

Gaudel, A., Cooper, O. R., Chang, K.-L., Bourgeois, I., Ziemke, J. R., Strode, S. A., Oman, L. D., Sellitto, P., Nédélec, P., Blot, R., et al.: Aircraft observations since the 1990s reveal increases of tropospheric ozone at multiple locations across the Northern Hemisphere, Science Advances, 6, eaba8272, 2020.

Gery, M. W., Whitten, G. Z., Killus, J. P., and Dodge, M. C.: A photochemical kinetics mechanism for urban and regional scale computer
640   modeling, Journal of Geophysical Research: Atmospheres, 94, 12 925–12 956, 1989.

Gorter, W., Van Angelen, J., Lenaerts, J., and Van den Broeke, M.: Present and future near-surface wind climate of Greenland from high resolution regional climate modelling, Climate dynamics, 42, 1595–1611, 2014.

Grell, G. A., Peckham, S. E., Schmitz, R., McKeen, S. A., Frost, G., Skamarock, W. C., and Eder, B.: Fully coupled "online" chemistry within the WRF model, Atmospheric Environment, 39, 6957–6975, 2005.

645   Guenther, A., Jiang, X., Heald, C., Sakulyanontvittaya, T., Duhl, T., Emmons, L., and Wang, X.: The Model of Emissions of Gases and Aerosols from Nature version 2.1 (MEGAN2. 1): an extended and updated framework for modeling biogenic emissions, 2012.

Halfacre, J., Knepp, T., Shepson, P., Thompson, C., Pratt, K., Li, B., Peterson, P., Walsh, S., Simpson, W., Matrai, P., et al.: Temporal and spatial characteristics of ozone depletion events from measurements in the Arctic, Atmospheric Chemistry and Physics, 14, 4875, 2014.

Hardacre, C., Wild, O., and Emberson, L.: An evaluation of ozone dry deposition in global scale chemistry climate models, Atmospheric
650   Chemistry and Physics, 15, 6419–6436, 2015.

Helmig, D., Ganzeveld, L., Butler, T., and Oltmans, S.: The role of ozone atmosphere-snow gas exchange on polar, boundary-layer tropospheric ozone? a review and sensitivity analysis, 2007a.

Helmig, D., Oltmans, S. J., Carlson, D., Lamarque, J.-F., Jones, A., Labuschagne, C., Anlauf, K., and Hayden, K.: A review of surface ozone in the polar regions, Atmospheric Environment, 41, 5138–5161, 2007b.

655   Helmig, D., Cohen, L. D., Bocquet, F., Oltmans, S., Grachev, A., and Neff, W.: Spring and summertime diurnal surface ozone fluxes over the polar snow at Summit, Greenland, Geophysical research letters, 36, 2009.

Helmig, D., Lang, E., Bariteau, L., Boylan, P., Fairall, C., Ganzeveld, L., Hare, J., Hueber, J., and Pallandt, M.: Atmosphere-ocean ozone fluxes during the TexAQS 2006, STRATUS 2006, GOMECC 2007, GasEx 2008, and AMMA 2008 cruises, Journal of Geophysical Research: Atmospheres, 117, 2012.

660   Hersbach, H., Bell, B., Berrisford, P., Hirahara, S., Horányi, A., Muñoz-Sabater, J., Nicolas, J., Peubey, C., Radu, R., Schepers, D., et al.: The ERA5 global reanalysis, Quarterly Journal of the Royal Meteorological Society, 2020.

29

Hines, K. M. and Bromwich, D. H.: Development and testing of Polar Weather Research and Forecasting (WRF) model. Part I: Greenland ice sheet meteorology, Monthly Weather Review, 136, 1971–1989, 2008.

Hong, S.-Y., Dudhia, J., and Chen, S.-H.: A revised approach to ice microphysical processes for the bulk parameterization of clouds and precipitation, Monthly weather review, 132, 103–120, 2004.

Iacono, M. J., Delamere, J. S., Mlawer, E. J., Shephard, M. W., Clough, S. A., and Collins, W. D.: Radiative forcing by long-lived greenhouse gases: Calculations with the AER radiative transfer models, Journal of Geophysical Research: Atmospheres, 113, 2008.

Inness, A., Ades, M., Agustí-Panareda, A., Barré, J., Benedictow, A., Blechschmidt, A.-M., Dominguez, J. J., Engelen, R., Eskes, H., Flemming, J., Huijnen, V., Jones, L., Kipling, Z., Massart, S., Parrington, M., Peuch, V.-H., Razinger, M., Remy, S., Schulz, M., and Suttie, M.: The CAMS reanalysis of atmospheric composition, Atmospheric Chemistry and Physics, 19, 3515–3556, https://doi.org/10.5194/acp-19-3515-2019, https://www.atmos-chem-phys.net/19/3515/2019/, 2019.

Janjić, Z. I.: The step-mountain eta coordinate model: Further developments of the convection, viscous sublayer, and turbulence closure schemes, Monthly weather review, 122, 927–945, 1994.

Janjić, Z. I.: Nonsingular implementation of the Mellor-Yamada level 2.5 scheme in the NCEP Meso model, 2001.

Janssens-Maenhout, G., Crippa, M., Guizzardi, D., Muntean, M., Schaaf, E., Dentener, F., Bergamaschi, P., Pagliari, V., Olivier, J., Peters, J., et al.: EDGAR v4.3.2 Global Atlas of the three major Greenhouse Gas Emissions for the period 1970–2012, Earth Syst. Sci. Data Discuss, 2017.

Kain, J. S.: The Kain–Fritsch convective parameterization: an update, Journal of applied meteorology, 43, 170–181, 2004.

Kavassalis, S. C. and Murphy, J. G.: Understanding ozone-meteorology correlations: A role for dry deposition, Geophysical Research Letters, 44, 2922–2931, 2017.

Klein, T., Heinemann, G., Bromwich, D. H., Cassano, J. J., and Hines, K. M.: Mesoscale modeling of katabatic winds over Greenland and comparisons with AWS and aircraft data, Meteorology and Atmospheric Physics, 78, 115–132, 2001.

Lana, A., Bell, T., Simó, R., Vallina, S., Ballabrera-Poy, J., Kettle, A., Dachs, J., Bopp, L., Saltzman, E., Stefels, J., et al.: An updated climatology of surface dimethylsulfide concentrations and emission fluxes in the global ocean, Global Biogeochemical Cycles, 25, 2011.

Law, K. S., Roiger, A., Thomas, J. L., Marelle, L., Raut, J.-C., Dalsøren, S., Fuglestvedt, J., Tuccella, P., Weinzierl, B., and Schlager, H.: Local Arctic air pollution: Sources and impacts, Ambio, 46, 453–463, 2017.

Lee, D. S., Holland, M. R., and Falla, N.: The potential impact of ozone on materials in the UK, Atmospheric Environment, 30, 1053–1065, 1996.

Lelieveld, J. and Dentener, F. J.: What controls tropospheric ozone?, Journal of Geophysical Research: Atmospheres, 105, 3531–3551, 2000.

Lin, M., Horowitz, L. W., Payton, R., Fiore, A. M., and Tonnesen, G.: US surface ozone trends and extremes from 1980 to 2014: quantifying the roles of rising Asian emissions, domestic controls, wildfires, and climate, Atmospheric Chemistry and Physics, 17, 2943–2970, 2017.

Lin, M., Malyshev, S., Shevliakova, E., Paulot, F., Horowitz, L. W., Fares, S., Mikkelsen, T. N., and Zhang, L.: Sensitivity of ozone dry deposition to ecosystem-atmosphere interactions: A critical appraisal of observations and simulations, Global Biogeochemical Cycles, 33, 1264–1288, 2019.

Lin, M., Horowitz, L. W., Xie, Y., Paulot, F., Malyshev, S., Shevliakova, E., Finco, A., Gerosa, G., Kubistin, D., and Pilegaard, K.: Vegetation feedbacks during drought exacerbate ozone air pollution extremes in Europe, Nature Climate Change, 10, 444–451, 2020.

Luhar, A. K., Galbally, I. E., Woodhouse, M. T., and Thatcher, M.: An improved parameterisation of ozone dry deposition to the ocean and its impact in a global climate-chemistry model, Atmospheric Chemistry and Physics, 17, 3749, 2017.

Luhar, A. K., Woodhouse, M. T., and Galbally, I. E.: A revised global ozone dry deposition estimate based on a new two-layer parameterisation for air-sea exchange and the multi-year MACC composition reanalysis., Atmospheric Chemistry & Physics, 18, 2018.

MacDonald, S., Gómez Martín, J., Chance, R., Warriner, S., Saiz-Lopez, A., Carpenter, L., and Plane, J.: A laboratory characterisation of inorganic iodine emissions from the sea surface: dependence on oceanic variables and parameterisation for global modelling, Atmospheric Chemistry and Physics, 14, 5841–5852, 2014.

Magi, L., Schweitzer, F., Pallares, C., Cherif, S., Mirabel, P., and George, C.: Investigation of the uptake rate of ozone and methyl hydroperoxide by water surfaces, The Journal of Physical Chemistry A, 101, 4943–4949, 1997.

Mahmood, R., von Salzen, K., Norman, A.-L., Galí, M., and Levasseur, M.: Sensitivity of Arctic sulfate aerosol and clouds to changes in future surface seawater dimethylsulfide concentrations., Atmospheric Chemistry & Physics, 19, 2019.

Marelle, L., Thomas, J. L., Raut, J.-C., Law, K. S., Jalkanen, J.-P., Johansson, L., Roiger, A., Schlager, H., Kim, J., Reiter, A., et al.: Air quality and radiative impacts of Arctic shipping emissions in the summertime in northern Norway: from the local to the regional scale, 2016.

Marelle, L., Raut, J.-C., Law, K. S., and Duclaux, O.: Current and Future Arctic Aerosols and Ozone From Remote Emissions and Emerging Local Sources—Modeled Source Contributions and Radiative Effects, Journal of Geophysical Research: Atmospheres, 123, 12–942, 2018.

Martino, M., Lézé, B., Baker, A. R., and Liss, P. S.: Chemical controls on ozone deposition to water, Geophysical research letters, 39, 2012.

Michou, M., Laville, P., Serça, D., Fotiadi, A., Bouchou, P., and Peuch, V.-H.: Measured and modeled dry deposition velocities over the ESCOMPTE area, Atmospheric Research, 74, 89–116, 2005.

Morris, J.: The aqueous solubility of ozone–A review, Ozone news, 1, 14–16, 1988.

Muller, J. B., Dorsey, J. R., Flynn, M., Gallagher, M. W., Percival, C. J., Shallcross, D. E., Archibald, A., Roscoe, H. K., Obbard, R. W., Atkinson, H. M., et al.: Energy and ozone fluxes over sea ice, Atmospheric environment, 47, 218–225, 2012.

Murray, K. A., Kramer, L. J., Doskey, P. V., Ganzeveld, L., Seok, B., Van Dam, B., and Helmig, D.: Dynamics of ozone and nitrogen oxides at Summit, Greenland. II. Simulating snowpack chemistry during a spring high ozone event with a 1-D process-scale model, Atmospheric Environment, 117, 110–123, 2015.

Nguyen, Q. T., Glasius, M., Sørensen, L. L., Jensen, B., Skov, H., Birmili, W., Wiedensohler, A., Kristensson, A., Nøjgaard, J. K., and Massling, A.: Seasonal variation of atmospheric particle number concentrations, new particle formation and atmospheric oxidation capacity at the high Arctic site Villum Research Station, Station Nord, 2016.

Nuvolone, D., Petri, D., and Voller, F.: The effects of ozone on human health, Environmental Science and Pollution Research, 25, 8074–8088, 2018.

Oh, I.-B., Byun, D. W., Kim, H.-C., Kim, S., and Cameron, B.: Modeling the effect of iodide distribution on ozone deposition to seawater surface, Atmospheric Environment, 42, 4453–4466, 2008.

Oltmans, S., Lefohn, A., Shadwick, D., Harris, J., Scheel, H., Galbally, I., Tarasick, D., Johnson, B., Brunke, E.-G., Claude, H., et al.: Recent tropospheric ozone changes–A pattern dominated by slow or no growth, Atmospheric Environment, 67, 331–351, 2013.

Paatero, J., Vaattovaara, P., Vestenius, M., Meinander, O., Makkonen, U., Kivi, R., Hyvärinen, A., Asmi, E., Tjernström, M., and Leck, C.: Finnish contribution to the arctic summer cloud ocean study (ASCOS) expedition, Arctic Ocean 2008, Geophysica, 45, 119–146, 2009.

Padro, J.: Summary of ozone dry deposition velocity measurements and model estimates over vineyard, cotton, grass and deciduous forest in summer, Atmospheric Environment, 30, 2363–2369, 1996.

Pausata, F., Pozzoli, L., Vignati, E., and Dentener, F.: North Atlantic Oscillation and tropospheric ozone variability in Europe: model analysis and measurements intercomparison., Atmospheric Chemistry & Physics, 12, 2012.

Pedregosa, F., Varoquaux, G., Gramfort, A., Michel, V., Thirion, B., Grisel, O., Blondel, M., Prettenhofer, P., Weiss, R., Dubourg, V., et al.: Scikit-learn: Machine learning in Python, the Journal of machine Learning research, 12, 2825–2830, 2011.

Porter, J., de Bruyn, W., Miller, S., and Saltzman, E.: Air/sea transfer of highly soluble gases over coastal waters, Geophysical Research Letters, 47, no–no, 2020.

740

Pound, R. J., Sherwen, T., Helmig, D., Carpenter, L. J., and Evans, M. J.: Influences of oceanic ozone deposition on tropospheric photochemistry, Atmospheric Chemistry and Physics Discussions, pp. 1–25, 2019.

Prados Roman, C., Cuevas, C. A., Fernandez, R. P., Kinnison, D. E., Lamarque, J. F., and Saiz-lopez, A.: A negative feedback between anthropogenic ozone pollution and enhanced ocean emissions of iodine, 2015.

745

Pratt, K. A., Custard, K. D., Shepson, P. B., Douglas, T. A., Pöhler, D., General, S., Zielcke, J., Simpson, W. R., Platt, U., Tanner, D. J., et al.: Photochemical production of molecular bromine in Arctic surface snowpacks, Nature Geoscience, 6, 351–356, 2013.

Reeser, D. I., Jammoul, A., Clifford, D., Brigante, M., D'Anna, B., George, C., and Donaldson, D.: Photoenhanced reaction of ozone with chlorophyll at the seawater surface, The Journal of Physical Chemistry C, 113, 2071–2077, 2009.

Riedel, A., Michel, C., Gosselin, M., and LeBlanc, B.: Winter–spring dynamics in sea-ice carbon cycling in the coastal Arctic Ocean, Journal of Marine Systems, 74, 918–932, 2008.

750

Schmale, J., Arnold, S., Law, K. S., Thorp, T., Anenberg, S., Simpson, W., Mao, J., and Pratt, K.: Local Arctic air pollution: A neglected but serious problem, Earth's Future, 6, 1385–1412, 2018.

Sherwen, T., Chance, R. J., Tinel, L., Ellis, D., Evans, M. J., and Carpenter, L. J.: A machine learning based global sea-surface iodide distribution, Earth System Science Data Discussions, pp. 1–40, 2019.

755

Silva, S. J. and Heald, C. L.: Investigating dry deposition of ozone to vegetation, Journal of Geophysical Research: Atmospheres, 123, 559–573, 2018.

Stefels, J., Steinke, M., Turner, S., Malin, G., and Belviso, S.: Environmental constraints on the production and removal of the climatically active gas dimethylsulphide (DMS) and implications for ecosystem modelling, Biogeochemistry, 83, 245–275, 2007.

Tarasick, D., Galbally, I. E., Cooper, O. R., Schultz, M. G., Ancellet, G., Leblanc, T., Wallington, T. J., Ziemke, J., Liu, X., Steinbacher,

760

M., et al.: Tropospheric Ozone Assessment Report: Tropospheric ozone from 1877 to 2016, observed levels, trends and uncertainties, Elementa: Science of the Anthropocene, 7, 2019.

Thomas, J. L., Stutz, J., Lefer, B., Huey, L. G., Toyota, K., Dibb, J. E., and von Glasow, R.: Modeling chemistry in and above snow at Summit, Greenland – Part 1: Model description and results, Atmospheric Chemistry and Physics, 11, 4899–4914, https://doi.org/10.5194/acp-11-4899-2011, https://acp.copernicus.org/articles/11/4899/2011/, 2011.

765

Thomas, J. L., Raut, J.-C., Law, K. S., Marelle, L., Ancellet, G., Ravetta, F., Fast, J. D., Pfister, G., Emmons, L. K., Diskin, G. S., Weinheimer, A., Roiger, A., and Schlager, H.: Pollution transport from North America to Greenland during summer 2008, Atmospheric Chemistry and Physics, 13, 3825–3848, https://doi.org/10.5194/acp-13-3825-2013, https://www.atmos-chem-phys.net/13/3825/2013/, 2013.

Thompson, C. R., Shepson, P. B., Liao, J., Huey, L. G., Cantrell, C., Flocke, F., and Orlando, J.: Bromine atom production and chain propagation during springtime Arctic ozone depletion events in Barrow, Alaska, Atmospheric Chemistry and Physics, 17, 3401, 2017.

770

Tjernstrom, M., Birch, C. E., Brooks, I. M., Shupe, M. D., Persson, P. O. G., Sedlar, J., Mauritsen, T., Leck, C., Paatero, J., Szczodrak, M., et al.: Meteorological conditions in the central Arctic summer during the Arctic Summer Cloud Ocean Study (ASCOS), Atmospheric Chemistry and Physics, 12, 6863–6889, 2012.

Toyota, K., McConnell, J., Staebler, R., and Dastoor, A.: Air–snowpack exchange of bromine, ozone and mercury in the springtime Arctic simulated by the 1-D model PHANTAS–Part 1: In-snow bromine activation and its impact on ozone, Atmos. Chem. Phys, 14, 4101–4133, 2014.

Toyota, K., Dastoor, A. P., and Ryzhkov, A.: Parameterization of gaseous dry deposition in atmospheric chemistry models: Sensitivity to aerodynamic resistance formulations under statically stable conditions, Atmospheric Environment, 147, 409–422, 2016.

Val Martin, M., Heald, C., and Arnold, S.: Coupling dry deposition to vegetation phenology in the Community Earth System Model: Implications for the simulation of surface O3, Geophysical Research Letters, 41, 2988–2996, 2014.

Van Dam, B., Helmig, D., Toro, C., Doskey, P., Kramer, L., Murray, K., Ganzeveld, L., and Seok, B.: Dynamics of ozone and nitrogen oxides at Summit, Greenland: I. Multi-year observations in the snowpack, Atmospheric Environment, 123, 268–284, 2015.

Van Dam, B., Helmig, D., Doskey, P. V., and Oltmans, S. J.: Summertime surface O3 behavior and deposition to tundra in the Alaskan Arctic, Journal of Geophysical Research: Atmospheres, 121, 8055–8066, 2016.

Wentz, F. and Meissner, T.: AMSR-E/Aqua Daily L3 Global Ascending/Descending .25x.25 deg Ocean Grids, Version 2., 2004.

Wesely, M.: Parameterization of surface resistances to gaseous dry deposition in regional-scale numerical models, Atmospheric Environment (1967), 23, 1293–1304, 1989.

Wesely, M. and Hicks, B.: A review of the current status of knowledge on dry deposition, Atmospheric environment, 34, 2261–2282, 2000.

Wild, O., Zhu, X., and Prather, M. J.: Fast-J: Accurate simulation of in-and below-cloud photolysis in tropospheric chemical models, Journal of Atmospheric Chemistry, 37, 245–282, 2000.

Wong, A. Y., Geddes, J. A., Tai, A. P., and Silva, S. J.: Importance of dry deposition parameterization choice in global simulations of surface ozone, Atmospheric Chemistry and Physics, 19, 14 365–14 385, 2019.

Yang, X., Blechschmidt, A.-M., Bognar, K., McClure-Begley, A., Morris, S., Petropavlovskikh, I., Richter, A., Skov, H., Strong, K., Tarasick, D. W., et al.: Pan-Arctic surface ozone: modelling vs. measurements, Atmospheric Chemistry and Physics, 20, 15 937–15 967, 2020.

Young, P. J., Naik, V., Fiore, A. M., Gaudel, A., Guo, J., Lin, M., Neu, J., Parrish, D., Rieder, H., Schnell, J., et al.: Tropospheric Ozone Assessment Report: Assessment of global-scale model performance for global and regional ozone distributions, variability, and trends, Elementa: Science of the Anthropocene, 6, 2018.

Zaveri, R. A. and Peters, L. K.: A new lumped structure photochemical mechanism for large-scale applications, Journal of Geophysical Research: Atmospheres, 104, 30 387–30 415, 1999.

Zeller, K.: Wintertime ozone fluxes and profiles above a subalpine spruce–fir forest, Journal of Applied Meteorology, 39, 92–101, 2000.

Zhou, P., Ganzeveld, L., Rannik, Ü., Zhou, L., Gierens, R., Taipale, D., Mammarella, I., and Boy, M.: Simulating ozone dry deposition at a boreal forest with a multi-layer canopy deposition model, Atmospheric Chemistry and Physics, 17, 1361–1379, 2017.